

Rigorous derivation of the triple scattering signal from single-atom responses

Vyacheslav Shatokhin and Thomas Wellens

Institute of Physics, University of Freiburg, Hermann-Herder-Str. 3, D-79104 Freiburg, Germany

(Dated: November 13, 2018)

We study coherent backscattering of intense laser light from three immobile two-level atoms using the master equation approach. The master equation is solved analytically, and the triple scattering spectrum is expressed in quadratures. We show that this solution can be obtained via a self-consistent combination of single-atom spectral responses, and is equivalent to the solution following from the diagrammatic pump-probe approach. We deduce the general expressions for single-atom building blocks which can be used in simulations of multiple inelastic scattering of laser light in the bulk atomic medium.

I. INTRODUCTION

Coherent backscattering (CBS) is an enhancement of the average intensity of the resonant wave backscattered off a dilute disordered medium due to the constructive interference between the counter-propagating multiply scattered amplitudes possessing time-reversal symmetry [1]. Recent experiments on CBS of light from cold atoms [2–6] studied the impact of the atomic internal structure on the phase coherence of the interfering waves. It was shown that the spin-flips of a photon on degenerate dipole transitions of rubidium atoms [2–4, 6], as well as nonlinear inelastic scattering from saturated strontium [5] and rubidium [6] atoms induced by intense laser field significantly reduce the enhanced backscattering. It should be mentioned that, besides the importance of its own, the studies of CBS of light by cold atoms are also motivated by the interest in photon localization [7, 8] and random lasing [9, 10] in dense atomic clouds.

Whereas there is a detailed description of CBS of light by atoms with arbitrary internal degeneracy in the elastic (linear) scattering regime [4, 11, 12], multiple inelastic scattering theory exists only for atoms weakly saturated by two photons [13]. But the parameter regimes of moderate or strong saturations probed in the experiments [5, 6] requires a non-perturbative treatment of the atom-laser field interactions, and is beyond the reach of the diagrammatic approach put forward in [13].

Standard non-perturbative quantum-optical methods, such as a master equation approach (see, for instance, [14–16]), can be used for a description of CBS of intense laser light from cold atoms. However, due to the exponential growth of the Hilbert space with increasing number of scatterers these methods are fundamentally limited to systems of a few scatterers. So far, the master equation approach and extensions thereof have been successfully applied to treat double scattering [17–20].

To avoid the above problem of the exponential growth of the Hilbert space, and yet to account for the atom-laser field interaction strength non-perturbatively, we proposed a stochastic method of solving the multiple scattering problem in dilute cold atomic clouds which we call the pump-probe approach to CBS [21, 22]. The main idea of this method is to express the multiple scattering signal through single-atom responses to a classi-

cal polychromatic random field, of which one component represents a laser (pump) field, while the remaining components describe weak (probe) fields scattered from the surrounding distant atoms.

So far, the validity of the pump-probe approach was proven in the case of double scattering by two two-level atoms [21, 22] by analytically establishing the equivalence with the results following from the master equation approach [23]. Furthermore, we showed that the expressions for the double scattering background and interference spectra can be represented graphically, by self-consistently combining single-atom building blocks [24]. Thus, the pump-probe approach is related to the non-perturbative methods of quantum optics, on the one hand, and to the diagrammatic scattering theories, on the other hand.

In the present contribution, we explore these relations further. Namely, from the rigorous solutions of the master equation for three two-level atoms we deduce the analytical expressions for the triple scattering background and interference spectra of CBS. We present our results diagrammatically by self-consistently combining single-atom building blocks, analogously to the case of double scattering [24]. Thereby, we show the equivalence between the master equation and the pump-probe approaches to CBS for triple scattering. Moreover, we deduce general expressions describing the spectral response of an atom subjected to an arbitrary number of probe fields. These expressions will be required in future work to implement the pump-probe approach for a medium consisting of an arbitrarily large number of atoms.

The structure of this paper is as follows. In the next section, we present the model, the master equation, and the main quantity of interest – the triple scattering contribution to CBS of light from three two-level atoms. In Sec. III we describe the method to find an analytical solution of the master equation which links it to the pump-probe approach. Sections IV and V contain our main results. They include diagrammatic expansions of single-atom building blocks into the elastic and inelastic spectral responses whose composition yields the ladder and crossed spectra (Sec. IV), and the general expressions for single-atom building blocks (Sec. V). We present analytical and numerical triple scattering spectra in Sec. VI. Conclusions of this work are presented in Sec. VII.

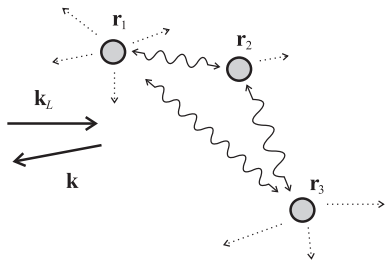


FIG. 1: Three atoms (gray circles) located in the radiation zone of each other are driven by a quasi-resonant laser field of arbitrary intensity with a wave-vector \mathbf{k}_L . They radiatively decay (dotted arrows) into a common electromagnetic bath, which also mediates the resonant dipole-dipole interaction (double wavy arrows). We will be interested in the far-field intensity of the scattered light along \mathbf{k} .

II. MODEL

A. Master equation

We will start out with introducing our model depicted in Fig. 1. It includes three quantum scatterers (two-level atoms) embedded in a common electromagnetic reservoir at fixed random positions \mathbf{r}_λ and excited by a quasi-resonant continuous wave laser field with a wave vector \mathbf{k}_L . We will be interested in the disorder-averaged far-field intensity of the light scattered into a given direction \mathbf{k} .

To describe CBS of light from three laser-driven atoms, we will employ the master equation approach [14, 16] which has already been used for calculating double scattering from two saturated Sr [17, 20] and two-level atoms [23]. Therefore, we will next present a master equation governing the evolution of the quantum mechanical expectation values of an arbitrary atomic observable Q of a three-atom system. In the Heisenberg picture and in the frame rotating at the laser frequency ω_L , $\langle Q \rangle$ obeys the following equation of motion [23]:

$$\begin{aligned} \langle \dot{Q} \rangle = & \sum_{\lambda=1}^3 \langle -i\delta[\sigma_\lambda^+ \sigma_\lambda^-, Q] - \frac{i}{2}[\Omega_\lambda \sigma_\lambda^+ + \Omega_\lambda^* \sigma_\lambda^-, Q] \\ & - \gamma(\sigma_\lambda^+ \sigma_\lambda^- Q + Q \sigma_\lambda^+ \sigma_\lambda^- - 2\sigma_\lambda^+ Q \sigma_\lambda^-) \rangle \\ & + \sum_{\lambda \neq \mu=1}^3 (T_{\lambda\mu} \langle [\sigma_\lambda^+ Q, \sigma_\mu^-] + T_{\lambda\mu}^* [\sigma_\lambda^+, Q \sigma_\mu^-] \rangle). \end{aligned} \quad (1)$$

Here, $\sigma_\lambda^- = |1\rangle_\lambda \langle 2|_\lambda$ and $\sigma_\lambda^+ = |2\rangle_\lambda \langle 1|_\lambda$, with $|1\rangle_\lambda$ and $|2\rangle_\lambda$ being respectively the ground and excited states of atom λ , denote the atomic lowering and raising operators. Furthermore, $\Omega_\lambda = \Omega e^{i\mathbf{k}_L \cdot \mathbf{r}_\lambda}$ is the Rabi frequency dependent on the atomic position \mathbf{r}_λ , $\delta = \omega_L - \omega_0$ is the laser-atom detuning, and γ is half the radiative decay rate of the excited state. The lower line of Eq. (1) describes the retarded dipole-dipole interaction proportional to the complex couplings $T_{\lambda\mu}$. The couplings $T_{\lambda\mu}$, in turn, are

inversely proportional to the distance between the atoms λ and μ :

$$T_{\lambda\mu} \equiv i \frac{3}{2} \gamma (1 - (\hat{\mathbf{d}} \cdot \hat{\mathbf{r}}_{\lambda\mu})^2) \frac{e^{-ik_L r_{\lambda\mu}}}{k_L r_{\lambda\mu}}, \quad (2)$$

where $\hat{\mathbf{d}}$ and $\hat{\mathbf{r}}_{\lambda\mu}$ are unit vectors along the atomic dipole moment and radius-vector connecting the atoms λ and μ , respectively, and $r_{\lambda\mu} = |\mathbf{r}_\lambda - \mathbf{r}_\mu|$. It should be stressed that Eq. (2) is valid only in the limit $k_L r_{\lambda\mu} \gg 1$, which is standard in the context of CBS, and is also assumed here. Note that although the constants $T_{\lambda\mu} = T_{\mu\lambda}$ and $T_{\lambda\mu}^* = T_{\mu\lambda}^*$, the interaction Liouvillians in Eq. (1) associated with these constants are not symmetric under the permutation of the indices λ and μ . Physically, they describe different excitation transfer processes induced by the far-field dipole-dipole interaction Liouvillian [23]. We will discuss this issue in Sec. III C 1.

B. Triple scattering intensity

Solution of Eq. (1) gives access to the expectation values of observables of the field radiated by a system of three atoms. We will focus on the triple scattering contribution to the stationary scattered light intensity in the direction of the wave vector \mathbf{k} . This quantity is a part of the general expression for the intensity of the scattered light given by

$$\langle I(\mathbf{k}) \rangle_{\text{ss}} = \sum_{\lambda} \langle \sigma_\lambda^+ \sigma_\lambda^- \rangle_{\text{ss}} + \sum_{\lambda, \mu \neq \lambda} \langle \sigma_\lambda^+ \otimes \sigma_\mu^- \rangle_{\text{ss}} e^{i\mathbf{k} \cdot (\mathbf{r}_\lambda - \mathbf{r}_\mu)}, \quad (3)$$

where the angular brackets $\langle \dots \rangle_{\text{ss}}$ denote the quantum-mechanical average in the steady state. The existence of the steady state is guaranteed by the fact that the corresponding expectation values in the right hand side of Eq. (3) are deduced from the solution of a linear equation (see Eq. (9) below) with a non-singular evolution matrix ($A + V$) whose eigenvalues have negative real parts. The first and second terms in Eq. (3) describe the incoherent (or background) and the interference intensities, respectively.

In the framework of the master equation approach, the multiple scattering contributions correspond to the subsequent terms in a perturbative expansion of the stationary solution of Eq. (1) in the power series of the dipole-dipole interaction constants. The first-order term, proportional to $|T_{\lambda\mu}|$, describes *the amplitude of double scattering* between the atoms λ and μ . Consequently, *the intensity of triple scattering* between atoms 1, 2 and 3 must be proportional to $|T_{12} T_{23}|^2$. Furthermore, the CBS signal is observed after the configuration, or disorder, averaging over the random positions of the scatterers, which will be denoted as $\langle \dots \rangle_{\text{conf}}$. Summarizing the above, we can write the expression for the triple scatter-

ing contribution to CBS as follows:

$$\begin{aligned} \langle\langle I(\mathbf{k}) \rangle\rangle_{\text{ss}}^{(4)} \rangle_{\text{conf}} &= \sum_{\lambda=1}^3 \langle\langle \sigma_{\lambda}^{+} \sigma_{\lambda}^{-} \rangle\rangle_{\text{ss}}^{(4)} \rangle_{\text{conf}} \\ &+ \sum_{\lambda, \mu \neq \lambda}^3 \langle\langle \sigma_{\lambda}^{+} \otimes \sigma_{\mu}^{-} \rangle\rangle_{\text{ss}}^{(4)} e^{i\mathbf{k} \cdot (\mathbf{r}_{\lambda} - \mathbf{r}_{\mu})} \rangle_{\text{conf}}, \end{aligned} \quad (4)$$

where the superscript (4) denotes the fourth order in the dipole-dipole coupling. Following the standard nomenclature in the field of coherent quantum transport [25], we will refer to the configuration averaged background and interference contributions as the ladder and crossed intensities, respectively.

In the following, we will ignore recurrent scattering, which is proportional to $|T_{\lambda\mu}|^4$. Although in a three-atom master equation, the recurrent and triple scattering contributions are of the same order of magnitude, in a dilute atomic cloud, the impact of the recurrent scattering on the observed signal scales as N^2 , and is by far dominated, for $N \gg 1$, by that of the triple scattering which scales as N^3 .

We will identify all triple scattering contributions which survive the disorder averaging. Since some of them are equal to each other, it will be sufficient to find only the non-equivalent contributions. To this end, in the next section we will study the structure and solutions of the master equation (1) in more detail.

III. SOLUTION OF THE MASTER EQUATION

A. Basis set of operators

Let us consider the evolution of the expectation value of an operator Q from the complete three-atom basis set of operators: $Q \in \{\vec{q}_1 \otimes \vec{q}_2 \otimes \vec{q}_3\}$, with

$$\begin{aligned} \vec{q}_{\lambda} &= (\mathbb{1}_{\lambda}, \sigma_{\lambda}^{-}, \sigma_{\lambda}^{+}, \sigma_{\lambda}^z)^T, \\ \mathbb{1}_{\lambda} &= \sigma_{\lambda}^{+} \sigma_{\lambda}^{-} + \sigma_{\lambda}^{-} \sigma_{\lambda}^{+}, \quad \sigma_{\lambda}^z = \sigma_{\lambda}^{+} \sigma_{\lambda}^{-} - \sigma_{\lambda}^{-} \sigma_{\lambda}^{+}. \end{aligned} \quad (5)$$

The normalization condition $\text{Tr}[\mathbb{1}_1 \otimes \mathbb{1}_2 \otimes \mathbb{1}_3 \rho] = 1$ which holds for any atomic density operator ρ reduces the size of the operator space by one, leading to a set of 63 operators. Their expectation values will be ordered as elements of the vector

$$\langle\vec{Q}\rangle = (\vec{x}, \vec{y}, \vec{z})^T, \quad (6)$$

with

$$\vec{x} = (\langle\vec{\sigma}_3\rangle, \langle\vec{\sigma}_2\rangle, \langle\vec{\sigma}_1\rangle)^T, \quad (7a)$$

$$\vec{y} = (\langle\vec{\sigma}_2 \otimes \vec{\sigma}_3\rangle, \langle\vec{\sigma}_1 \otimes \vec{\sigma}_3\rangle, \langle\vec{\sigma}_1 \otimes \vec{\sigma}_2\rangle)^T, \quad (7b)$$

$$\vec{z} = \langle\vec{\sigma}_1 \otimes \vec{\sigma}_2 \otimes \vec{\sigma}_3\rangle, \quad (7c)$$

where $\langle\vec{\sigma}_{\lambda}\rangle$ is a Bloch vector corresponding to atom λ :

$$\langle\vec{\sigma}_{\lambda}\rangle = (\langle\sigma_{\lambda}^{-}\rangle, \langle\sigma_{\lambda}^{+}\rangle, \langle\sigma_{\lambda}^z\rangle)^T. \quad (8)$$

The evolution of the vector $\langle\vec{Q}\rangle$ is governed by the equation of motion:

$$\dot{\langle\vec{Q}\rangle} = (A + V)\langle\vec{Q}\rangle + \vec{\Lambda}, \quad (9)$$

where the matrices A and V govern the dynamics of independent and dipole-dipole interacting atoms, respectively, and the vector $\vec{\Lambda}$ is given by Eq. (A4) in Appendix A.

The steady state solution of Eq. (9) which is of the fourth order in the matrix V reads:

$$\langle\vec{Q}\rangle_{\text{ss}}^{(4)} = (GV)^4 G\vec{\Lambda}, \quad (10)$$

where $G \equiv -A^{-1}$. Given the matrices A , V , and $\vec{\Lambda}$, it is easy to find $\langle\vec{Q}\rangle_{\text{ss}}^{(4)}$ numerically for any random positions \mathbf{r}_i of the atoms. Averaging this result over disorder gives $\langle\langle\vec{Q}\rangle\rangle_{\text{ss}}^{(4)} \rangle_{\text{conf}}$ and, consequently, the terms from the right hand side of Eq. (4) contributing to the ladder and crossed intensities. However, in this work we would like to prove the equivalence of the results of the master equation and the pump-probe approaches. Therefore, we will adhere to the analytical tools developed in [23, 24]. As will be seen below in Sec. V, using the analytical methods will enable us not only to prove the equivalence between the two methods, but also to deduce the general expressions for the single-atom building blocks which will be required in the future treatment of the multiple scattering of laser light in cold atomic clouds.

We will proceed with discussing the structure of the evolution matrices and presenting the recurrence relations connecting the steady-state vectors \vec{x} , \vec{y} , and \vec{z} .

B. Recurrence relations

For a vector $\langle\vec{Q}\rangle$ given by Eq. (6), the matrices A and V have the following block structure (see Appendix A):

$$A = \begin{pmatrix} M_{+} & 0 & 0 \\ L_{+} & M_{\times} & 0 \\ 0 & L_{\times} & N_{\times} \end{pmatrix}, \quad V = \begin{pmatrix} 0 & U_{\gamma} & 0 \\ U_{\perp} & U_{\times} & W_{\gamma} \\ 0 & W_{\perp} & W_{\times} \end{pmatrix}. \quad (11)$$

A perturbative expansion of the steady-state solution of Eq. (9) in the power series of the matrix V yields a system of coupled recurrence relations for the vectors $\vec{x}^{(n)}$, $\vec{y}^{(n)}$, and $\vec{z}^{(n)}$:

$$\vec{x}^{(n)} = G_{+} U_{\gamma} \vec{y}^{(n-1)}, \quad (12a)$$

$$\begin{aligned} \vec{y}^{(n)} &= G_{\times} U_{\perp} \vec{x}^{(n-1)} + G_{\times} U_{\times} \vec{y}^{(n-1)} + G_{\times} L_{+} \vec{x}^{(n)} \\ &+ G_{\times} W_{\gamma} \vec{z}^{(n-1)}, \end{aligned} \quad (12b)$$

$$\vec{z}^{(n)} = D_{\times} W_{\perp} \vec{y}^{(n-1)} + D_{\times} W_{\times} \vec{z}^{(n-1)} + D_{\times} L_{\times} \vec{y}^{(n)}, \quad (12c)$$

with the initial conditions determined by $\langle \vec{Q} \rangle_{ss}^{(n)} = 0$ for $n < 0$, and $\langle \vec{Q} \rangle_{ss}^{(0)} = (\vec{x}^{(0)}, \vec{y}^{(0)}, \vec{z}^{(0)})^T$, where

$$\vec{x}^{(0)} = (\langle \vec{\sigma}_3 \rangle^{(0)}, \langle \vec{\sigma}_2 \rangle^{(0)}, \langle \vec{\sigma}_1 \rangle^{(0)})^T, \quad (13a)$$

$$\vec{y}^{(0)} = (\langle \vec{\sigma}_2 \rangle^{(0)} \otimes \langle \vec{\sigma}_3 \rangle^{(0)}, \langle \vec{\sigma}_1 \rangle^{(0)} \otimes \langle \vec{\sigma}_3 \rangle^{(0)}, \langle \vec{\sigma}_1 \rangle^{(0)} \otimes \langle \vec{\sigma}_2 \rangle^{(0)})^T, \quad (13b)$$

$$\vec{z}^{(0)} = \langle \vec{\sigma}_1 \rangle^{(0)} \otimes \langle \vec{\sigma}_2 \rangle^{(0)} \otimes \langle \vec{\sigma}_3 \rangle^{(0)}, \quad (13c)$$

and $\langle \vec{\sigma}_\lambda \rangle^{(0)} = G_\lambda \vec{L}$. In Eqs. (12) and (13), we introduced a shorthand notation $G_\lambda \equiv G_\lambda(0)$ ($\lambda = 1, 2, 3$), $G_\alpha \equiv G_\alpha(0)$ ($\alpha = +, \times$), $D_\times \equiv D_\times(0)$, where

$$G_\lambda(z) = \frac{1}{z - M_\lambda}, \quad G_\alpha(z) = \frac{1}{z - M_\alpha}, \quad D_\times(z) = \frac{1}{z - N_\times}, \quad (14)$$

are the Green's matrices.

The possibility of demonstrating the equivalence between the results of the master equation and the pump-probe approach is based on the analytical solution of the recurrence relations (12) for fixed atomic positions, and on the subsequent analytical configuration averaging procedure.

In the following, we will identify the triple scattering paths for which configuration averaging of $\vec{x}^{(4)}$ and $\vec{y}^{(4)}$ yields the non-vanishing contributions around the backwards direction $\mathbf{k} = -\mathbf{k}_L$.

C. Selection of triple scattering paths

1. Interaction matrices and amplitudes of excitation transfer

In the framework of the master equation approach, multiple scattering paths can be defined according to the physical meaning of the interaction matrix V as describing the excitation transfer processes between the atoms [23]. This matrix can be decomposed into a sum

$$V = \sum_{\lambda \neq \mu=1}^3 (V_{\lambda\mu} + V_{\lambda\mu}^*), \quad (15)$$

with $V_{\lambda\mu} \propto T_{\lambda\mu}$ and $V_{\lambda\mu}^* \propto T_{\lambda\mu}^*$. Each term in the right hand side of Eq. (15) has the same block structure as the matrix V itself (that is, given by Eq. (11)), and generates an amplitude for a particular excitation transfer process between the atoms λ and μ (see Fig. 2). This amplitude corresponds to a propagation of the positive- (solid arrow) or negative-frequency (dashed arrow) field between the atoms [23]. Accordingly, the block matrices $(U_{\lambda\mu}^*)_\alpha$, $(W_{\lambda\mu}^*)_\alpha$ ($\alpha = \uparrow, \downarrow, \times$) are associated with a propagation of the positive-, and $(U_{\lambda\mu})_\alpha$, $(W_{\lambda\mu})_\alpha$ with the negative-frequency amplitude between the atoms λ and μ .

After the disorder averaging, those triple scattering processes which can be reduced to each other by relabeling the atomic indices result in identical contributions.

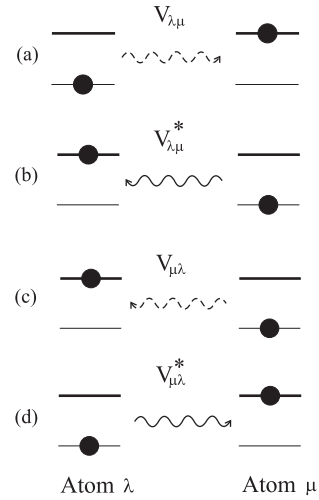


FIG. 2: Elementary excitation transfer processes between atoms λ and μ generated by the dipole-dipole interaction matrix V . Black spots correspond to the atomic states after the exchange process has occurred, and solid (dashed) arrows – to positive (negative) frequency amplitudes. The positive (negative) frequency amplitude of a transfer process from atom λ to atom μ is described by the matrix $V_{\mu\lambda}^*$ (d) ($V_{\lambda\mu}$ (a)), while the reversed process is described by matrix $V_{\lambda\mu}^*$ (b) ($V_{\mu\lambda}$ (c)).

Therefore, it is instructive to identify distinct types of triple scattering paths and consider one representative thereof. The intensity (4) then follows after multiplying the expression corresponding to a given type of triple scattering process by the number of times it occurs.

Without restricting the generality, subsequently we will be concerned with the triple scattering processes whose positive frequency amplitudes include the path $\mathbf{r}_1 \rightarrow \mathbf{r}_2$, and are thus proportional to T_{21}^* . It is easy to see that there are two triple scattering positive-frequency amplitudes containing the scattering process $\mathbf{r}_1 \rightarrow \mathbf{r}_2$: $\mathbf{r}_1 \rightarrow \mathbf{r}_2 \rightarrow \mathbf{r}_3$ and $\mathbf{r}_1 \rightarrow \mathbf{r}_2 \leftarrow \mathbf{r}_3$. The first and second amplitudes are proportional to $T_{21}^* T_{32}^*$ and $T_{21}^* T_{23}^*$, respectively.

Because the atomic positions are random, the dipole-dipole coupling constants (see Eq. (2)) carry random phases $e^{ik_L r_{\lambda\mu}}$, for which we assume, since $k_L r_{\lambda\mu} \gg 1$ as stated above, a uniform distribution between 0 and 2π . Then, to survive the disorder averaging, the positive-frequency triple scattering amplitudes must be combined with corresponding negative-frequency (conjugate) amplitudes. On top of that, the interference terms in Eq. (4) have additional, \mathbf{k} -sensitive random phases. This imposes further restrictions on the conjugate amplitudes.

For a given set of four interaction matrices describing a particular triple scattering process there are $4! = 24$ different terms (due to the non-commutativity of the matrices). Fortunately, the phase of each of these 24 terms is the same. Therefore, to see whether a given process survives the configuration averaging it suffices to consider only one term.

Using the above restrictions and analyzing different

triple scattering processes, we have identified four non-equivalent contributions which survive the configuration averaging: two ladder and two crossed contributions. Below, we will discuss them separately.

2. Ladder intensity

The ladder intensity is given by the first line in the right hand side of Eq. (4). We established that either of the two positive-frequency triple scattering processes, $\mathbf{r}_1 \rightarrow \mathbf{r}_2 \rightarrow \mathbf{r}_3$ and $\mathbf{r}_1 \rightarrow \mathbf{r}_2 \leftarrow \mathbf{r}_3$, can be combined with one negative-frequency triple scattering process, to yield a phase-independent contribution.

For the first excitation transfer process, proportional to $T_{21}^* T_{32}^*$ and generated by matrices V_{21}^* , V_{32}^* , the conjugate amplitude is generated by matrices V_{12} , V_{23} , and leads to a phase-independent solution for $\langle \sigma_3^+ \sigma_3^- \rangle_{\text{ss}}^{(4)}$. The corresponding triple scattering process which is composed of the co-propagating complex conjugate amplitudes, is shown in Fig. 3(a). Here, atom 3 is the source of the backscattered signal, depicted by one dashed and one solid arrows which are associated with the operators σ^+ and σ^- , respectively.

By simply exchanging the atomic indices 1, 2, 3, it is easy to see that the total number of triple scattering processes which yield the equivalent expressions upon the disorder averaging is equal to $3! = 6$.

Analyzing the second type of the triple scattering process which is generated by matrices V_{21}^* , V_{23}^* , we identified that, the only conjugate process which leads to a contribution to the ladder intensity is generated by matrices V_{12} and V_{32} . This triple scattering process results in a phase-independent solution for $\langle \sigma_2^+ \sigma_2^- \rangle^{(4)}$, and is depicted in Fig. 3(b). Since the corresponding term is symmetric with respect to a permutation between the indices of the outside atoms, there are in total 3 contributions of this type.

Combining the contributions of both types, which we call ‘‘ladder type 1’’ and ‘‘ladder type 2’’ in the following, we obtain the following expression for the total ladder intensity

$$L_{\text{tot}}^{(3)} = L_{\text{tot},1}^{(3)} + L_{\text{tot},2}^{(3)}, \quad (16)$$

with

$$L_{\text{tot},1}^{(3)} = 6 \langle \langle \sigma_3^+ \sigma_3^- \rangle \rangle_{\text{conf}}^{(4)}, \quad L_{\text{tot},2}^{(3)} = 3 \langle \langle \sigma_2^+ \sigma_2^- \rangle \rangle_{\text{conf}}^{(4)}, \quad (17)$$

where, from now on, we will for brevity drop the subscript ‘‘ss’’ in quantum mechanical steady state averages. Furthermore, the total ladder intensity splits into an elastic and an inelastic component:

$$L_{\text{tot},1}^{(3)} = L_{\text{el},1}^{(3)} + L_{\text{inel},1}^{(3)}, \quad L_{\text{tot},2}^{(3)} = L_{\text{el},2}^{(3)} + L_{\text{inel},2}^{(3)}, \quad (18)$$

where the elastic component results from factorizing the expectation value in Eq. (17), i.e.,

$$L_{\text{el},1}^{(3)} = 6 \langle \langle \sigma_3^+ \rangle \rangle_{\text{conf}} \langle \langle \sigma_3^- \rangle \rangle_{\text{conf}}^{(4)}, \quad (19)$$

and similarly for $L_{\text{el},2}^{(3)}$. The non-factorizable inelastic remainder $L_{\text{inel},i}^{(3)} = L_{\text{tot},i}^{(3)} - L_{\text{el},i}^{(3)}$, $i = 1, 2$, finally, is obtained as an integral over the frequency ν of the detected photon:

$$L_{\text{inel},i}^{(3)} = \int_{-\infty}^{\infty} d\nu L_{\text{inel},i}^{(3)}(\nu), \quad i = 1, 2, \quad (20)$$

where the spectrum $L_{\text{inel},i}^{(3)}(\nu)$ results from the Fourier transform of the non-factorizable part of the corresponding atomic correlation function $\langle \sigma^+(t+\tau)\sigma^-(t) \rangle - \langle \sigma^+(t+\tau) \rangle \langle \sigma^-(t) \rangle$ occurring in Eq. (17) with respect to τ .

3. Crossed intensity

Let us start discussing the crossed intensity by considering the processes $\propto T_{21}^* T_{32}^*$. In accordance with our interpretation of the excitation transfer processes and their association with the atomic raising and lowering operators, atom 3 now emits a positive frequency amplitude contributing to the CBS signal (solid arrow). Correspondingly, the negative frequency amplitudes (dashed arrows) of the outgoing field can be emitted either by atoms 1 or 2. Therefore, there are two types of two-atom correlation functions, $\langle \sigma_1^+ \otimes \sigma_3^- \rangle^{(4)}$ and $\langle \sigma_2^+ \otimes \sigma_3^- \rangle^{(4)}$, which contribute to the interference intensity, and will be called ‘‘crossed type 1’’ and ‘‘crossed type 2’’ in the following.

As follows from Eq. (4), the atomic dipole correlation function $\langle \sigma_1^+ \otimes \sigma_3^- \rangle^{(4)}$ (type 1) contributes to the CBS signal upon the configuration averaging if it includes the position-dependent phase factor which cancels itself with the phase $\exp(i\mathbf{k} \cdot \mathbf{r}_{13})$. We found that this happens only for the counter-propagating amplitudes which are proportional to $T_{21}^* T_{32}^* T_{12} T_{32}$ (Fig. 3(c)). In this case, the function $\langle \sigma_1^+ \otimes \sigma_3^- \rangle^{(4)}$ carries the phase $\exp(i\mathbf{k}_L \cdot \mathbf{r}_{13})$ and, hence, the interference term survives the configuration averaging in the exact backscattering direction (that is, for $\mathbf{k} = -\mathbf{k}_L$ [26]). A contribution of such counter-propagating amplitudes to the backscattered signal is generic for the CBS effect [25].

The term $\langle \sigma_2^+ \otimes \sigma_3^- \rangle^{(4)}$ (type 2) leads to another type of crossed contribution. It survives the disorder averaging in the backwards direction for the scattering process $\propto T_{21}^* T_{32}^* T_{12} T_{32}$. For this contribution, the negative frequency amplitude connecting atoms 2 and 3 is reversed (see Fig. 3(d)), whereas the one connecting atoms 1 and 2 is co-propagating with the positive-frequency amplitude. Such a type of interference processes is characteristic also for CBS from nonlinear classical scatterers [13, 27].

Last but not least, there is an interference contribution whose positive-frequency amplitude is proportional to $T_{21}^* T_{23}^*$. The diagram for the corresponding triple scattering process which survives the disorder average can be obtained from the diagram in Fig. 3(d) by substituting each solid arrow by a dashed one and vice versa. As the corresponding correlation function, $\langle \sigma_3^+ \otimes \sigma_2^- \rangle^{(4)}$, is the

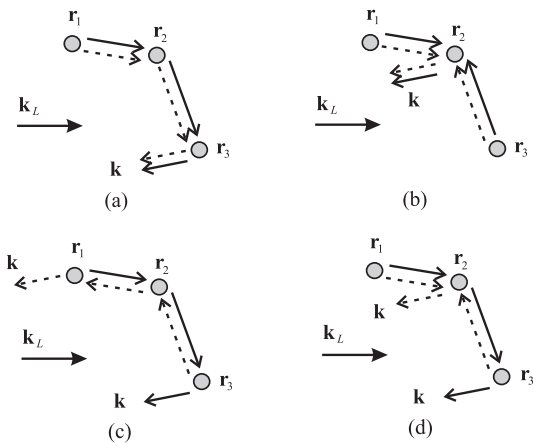


FIG. 3: Triple scattering processes surviving disorder averaging. Co-propagating amplitudes in diagrams (a) and (b), called “ladder type 1” and “ladder type 2”, in the following, have no overall phase and contribute to the background intensity; (c) interference of counter-propagating amplitudes between atoms 1 and 3 (“crossed type 1”), and (d) interference of amplitudes resulting from reversal of the amplitudes connecting atoms 2 and 3, carry phase factors $\exp\{i(\mathbf{k} + \mathbf{k}_L) \cdot \mathbf{r}_{13}\}$ and $\exp\{i(\mathbf{k} + \mathbf{k}_L) \cdot \mathbf{r}_{23}\}$ (“crossed type 2”), respectively (see Eq. (21) and preceding discussion), and thus contribute only in backscattering direction $\mathbf{k} = -\mathbf{k}_L$ where these phases vanish.

complex conjugate of the expression corresponding to a diagram in Fig. 3(d), its contribution can be accounted for by taking twice the real part of the expression describing Fig. 3(d).

Finally, by noting that the degeneracy of each of the crossed contributions is equal to $3! = 6$, we can write

$$C_{\text{tot}}^{(3)} = C_{\text{tot},1}^{(3)} + C_{\text{tot},2}^{(3)}, \quad (21)$$

with

$$C_{\text{tot},1}^{(3)} = 6 \langle \langle \sigma_1^+ \otimes \sigma_3^- \rangle \rangle^{(4)} e^{i\mathbf{k} \cdot \mathbf{r}_{13}} \rangle_{\text{conf}}, \quad (22)$$

$$C_{\text{tot},2}^{(3)} = 12 \text{Re} [\langle \langle \sigma_2^+ \otimes \sigma_3^- \rangle \rangle^{(4)} e^{i\mathbf{k} \cdot \mathbf{r}_{23}} \rangle_{\text{conf}}]. \quad (23)$$

Like in the ladder case, also the crossed intensity splits into an elastic and inelastic component $C_{\text{tot},i}^{(3)} = C_{\text{el},i}^{(3)} + C_{\text{inel},i}^{(3)}$, $i = 1, 2$, defined as the factorizable and non-factorizable components of the atomic correlation function.

IV. DIAGRAMMATIC REPRESENTATION OF THE TRIPLE SCATTERING CONTRIBUTION

Our goal is to obtain analytical expressions for the triple scattering ladder and crossed intensities defined in the previous Sec. III C, and to present them as compounds of single-atom spectral response functions. Since the derivation of these single-atom response functions starting from the master equation amounts to a quite

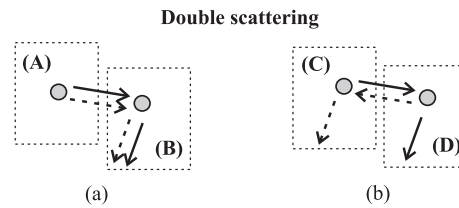


FIG. 4: Single-atom blocks contributing to double scattering. (a) Background and (b) interference contributions. Dashed frames subdivide multiple scattering contributions into single-atom building blocks.

lengthy calculation, we will, for the sake of clarity, first introduce the diagrammatic representation of the single-atom response functions and define the rules according to which these single-atom building blocks are connected with each other, before showing that the thereby diagrammatically obtained triple scattering signals are equivalent to the expressions derived from the master equation.

A. Triple vs. double scattering

For this purpose, let us recall the case of double scattering. Here, a diagrammatic representation in terms of single-atom building blocks has already been introduced [21, 22, 24] and been proven to be equivalent with the double scattering signal derived from the master equation [23]. We will therefore use this insight in order to construct analogous diagrams for the case of triple scattering.

1. Multiple scattering as a combination of single-atom responses

To start with, we plot the fundamental processes which survive the disorder average for the double and triple scattering contributions in Figs. 4 and 5, respectively.

Let us consider the diagrams in Fig. 4 which depict the configuration averaged (a) background and (b) interference contributions for double scattering. Here and henceforth the laser field is not displayed, in order to lighten the diagrams. As shown in [21, 22], both the ladder and crossed spectra can be obtained by combining single-atom building blocks which are enclosed in dashed frames (A)-(D) in Fig. 4(a), (b). The interaction between the atoms is accounted for perturbatively via the fictitious classical probe fields (solid and dashed arrows) which are connecting the atoms. These fictitious fields represent the far-field dipole-dipole interaction between the atoms [23]. Building block (A) is of the zeroth order, blocks (C), (D) of first, and block (B) of second order in the probe field or, equivalently, the dipole-dipole coupling strength. Figure 5 shows the composition of the configuration averaged triple scattering diagrams using single-atom build-

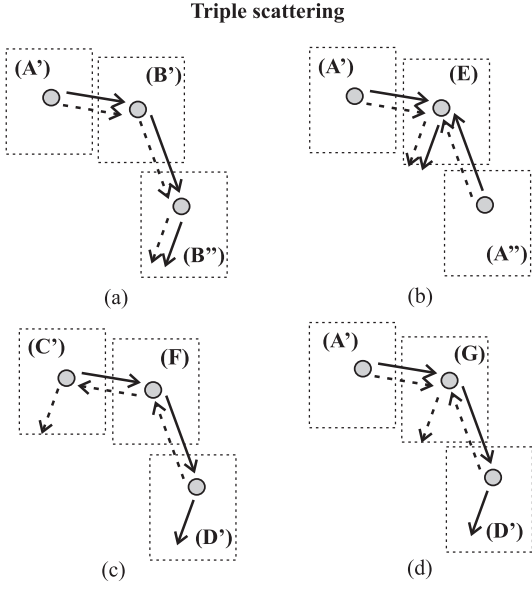


FIG. 5: Single-atom blocks contributing to triple scattering. (a) and (b) background; (c) and (d) interference contributions (corresponding to Fig. 3(a), (b), (c), and (d), respectively). Dashed frames subdivide multiple scattering contributions into single-atom building blocks.

ing blocks enclosed in dashed frames. Comparing the dashed frames in Figs. 4 and 5 we impose the compatibility conditions: $(A')=(A'')=(A)$, $(B')=(B'')=(B)$, $(C')=(C)$, and $(D')=(D)$.

This simple analysis allows us to fully specify the structure of the contribution to the ladder spectrum described by Fig. 5(a). It can be compounded from the building blocks (A) and (B) which can be found by solving the optical Bloch equations (OBE) under a classical *bichromatic* driving [21, 22].

The second ladder contribution, Fig. 5(b), as well as the crossed diagrams, Fig. 5(c) and (d), contain three new building blocks, (E), (F), and (G), respectively. These blocks describe the spectral response of the intermediate atom, which receives probe fields from its two neighbors. Therefore, within the pump-probe approach the blocks (E), (F), and (G) can be determined by solving the OBE under a classical *trichromatic* driving field.

Because the blocks (A), (B), (C), and (D) familiar from the treatment of double scattering are important also for triple scattering, we will next recall the corresponding single-atom spectral responses.

2. Diagrammatic pump-probe approach for double scattering

It is convenient to represent the solutions of the OBE under a bichromatic driving from which the single-atom building blocks (A), (B), (C), and (D) (see Fig. 4) are deduced diagrammatically [24], as displayed in Fig. 6.

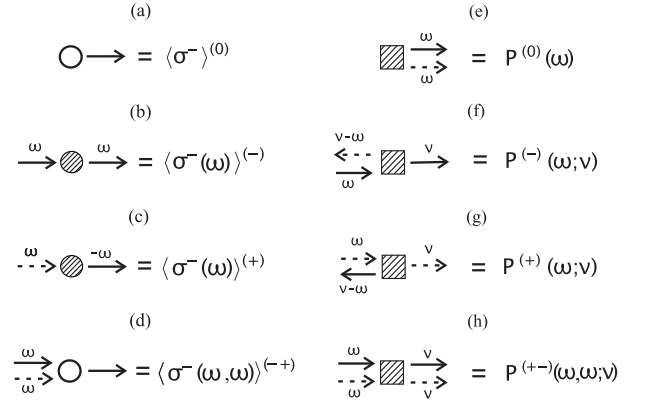


FIG. 6: Full set of elementary single-atom building blocks for the double scattering contribution. Circles are (hatched) blank if the frequency of the outgoing arrow is (different from) equal to the laser frequency. (a) Complex scattering amplitudes expressed through the induced atomic dipole moment and (b)-(d) corrections thereof due to the incoming probe fields; (e)-(f) Building blocks associated with the atomic dipole correlation functions describing inelastic scattering. In the response functions on the right hand side, the superscripts (0), (+), (-) and (+-) or (-+) correspond to the number and type (solid or dashed) of incoming arrows.

Any elastic and inelastic spectral response function describing the building blocks (A)-(D) can be compounded from circles and boxes shown in Fig. 6. Circles are associated with expectation values of the atomic dipole moment, and boxes with Laplace transforms of the steady-state atomic dipole temporal correlation functions [24]. Both types of the averages are evaluated perturbatively to second order in the weak probe field, which is represented by the incoming arrows in Fig. 6. The corresponding mathematical expressions are given in Sec. V.

Hatching the boxes and some of the circles indicates that the outgoing arrows have non-zero detunings from the laser frequency. This helps us to identify the frequencies of the outgoing arrows in the composition of the double scattering diagrams shown in Fig. 4(a),(b) – by virtue of the physical interpretation of the elementary building blocks as the effective nonlinear susceptibilities [24] which was partially inspired by the earlier work of Mollow [28, 29].

In all diagrams in Fig. 6, the important information about the incoming and outgoing arrows is encoded in their type (dashed or solid), direction (incoming or outgoing), and frequency (more precisely, the detuning from the laser frequency). By convention, we do not label the arrows that are on-resonant with the laser frequency. The notation of the spectral response functions on the right hand side of each diagram in Fig. 6 embodies the relevant information about the shapes and arrows of the elementary blocks, and is explained in detail in Sec. V.

In general, the diagrams in Fig. 6 correspond to the complex-valued spectral response functions. Their conjugate diagrams are obtained by replacements of each solid

arrow by a dashed one and vice versa. To obtain the corresponding spectral response functions, we must flip all signs in the symbolic definitions thereof. For instance, $(\langle \sigma^-(\omega, \omega) \rangle^{(-+)*})^* = \langle \sigma^+(\omega, \omega) \rangle^{(+ -)} = \langle \sigma^+(\omega, \omega) \rangle^{(-+)}$, where the latter equality follows because the incoming arrows are frequency-degenerate. By the same token, $(P^{(+)}(\omega; \nu))^* = P^{(-)}(\omega; \nu)$, whereas $P^{(+ -)}(\omega, \omega; \nu) = P^{(-+)}(\omega, \omega; \nu)$ is a real function.

How to compose the building blocks (A)-(D) from the elementary diagrams shown in Fig. 6 was discussed in Ref. [24]. The same setting will be generalized below in Sec. IV to describe spectral response functions with arbitrary number of the probe fields.

B. Ladder contribution

1. Type 1

The terms yielding the ladder spectrum of type 1 are shown in Fig. 7 in the form of three graphical equations. The left hand sides of these equations depict the single-atom building blocks (A), (B), (B) from Fig. 5(a). To allow for an easy identification of the fields contributing to the detected signal, here and henceforth the arrows representing the backscattered fields are directed downwards. Apart from this distinction, which becomes important when combining the single-atom responses into triple scattering contributions, the two building blocks (B) in Fig. 7 are equivalent.

The right hand sides of the graphical equations from Fig. 7 are the expansions of the building blocks into sums of the elastic and inelastic spectral response functions shown in Fig. 6. The arrows are not labeled by the frequency values in Fig. 7, because these values are uniquely defined at the stage of self-consistent combination of the single-atom responses into triple scattering diagrams (see below Sec. IV D).

Each of the elastic responses is depicted as a product (denoted by ‘ \times ’) of two elementary building blocks from Fig. 6(a-d) (as well as their complex conjugates). There are 2^n such products – the number of ways in which n incoming arrows can be distributed among the two circles. Last but not least, every building block contains one elementary inelastic building block depicted by a hatched box. The boxes (a2) and (b5) in Fig. 7 correspond to diagrams of Fig. 6(e) and (h), respectively.

Thus, the block (A) is equal to a sum of 2 terms, whereas the block (B) is equal to a sum of 5 terms. Consequently, a compound (A)(B)(B) yields the expression for the ladder intensity $L_{\text{tot},1}^{(3)}$ of type 1, see Eq. (17), consisting of 50 terms. Note that, as discussed in Sec. III C 2, see Eq. (17), the sum of these terms must be multiplied with a factor 6 in order to account for all different possibilities of exchanging the three atoms with each other.

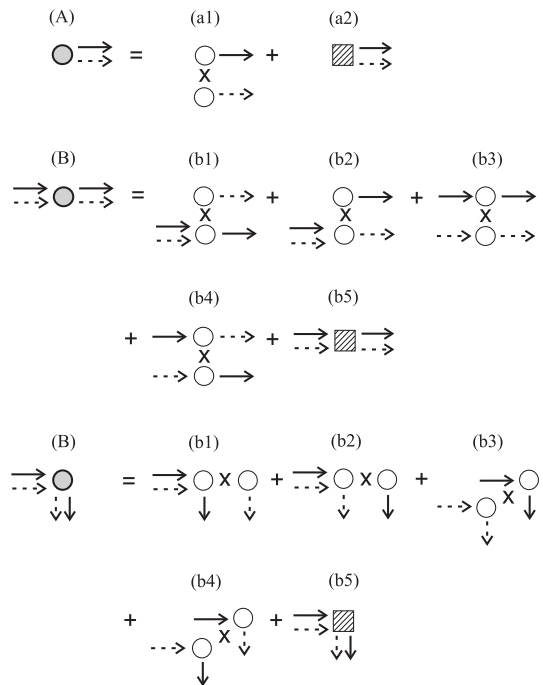


FIG. 7: (Left) single-atom building blocks contributing to the ladder spectrum of type 1; (right) expansion of the single-atom building blocks in elementary single-atom building blocks (see Fig. 6). Circles and boxes describe the elastic and inelastic responses, respectively. The backscattered signal is depicted by the downward arrows.

2. Type 2

To obtain this contribution, we perform a diagrammatic expansion of Fig. 5(b) into elementary single-atom building blocks, as shown in Fig. 8. Since the middle atom receives four arrows, the decomposition of the elastic response functions consists of $2^4 = 16$ terms, see Fig. 8(e1-e16).

Obviously, some of the elementary blocks in Fig. 8 describing the response of the middle atom, in particular, those with more than 2 incoming arrows and some with 2 incoming arrows, are not present in Fig. 6. Therefore, we depict in Fig. 9 the new spectral response functions required for describing the building block (E). All elementary blocks in Fig. 9 contain incoming arrows which originate from different atoms. Therefore, in general, the values of the incoming frequencies ω_1 and ω_2 are not equal to each other. In the framework of the pump-probe approach, the evaluation of the corresponding spectral response functions requires solving single-atom OBE under a classical trichromatic driving. In the degenerate case $\omega_1 = \omega_2 = \omega$, the functions $\langle \sigma^\pm(\omega_1, \omega_2) \rangle^{(-+)}$ are reduced to the functions $\langle \sigma^\pm(\omega, \omega) \rangle^{(-+)}$ familiar from double scattering (see Fig. 6).

Now, all elementary building blocks in Fig. 8 can be expressed in terms of the elementary building blocks shown in Figs. 6 and 9 or in terms of their complex conjugate

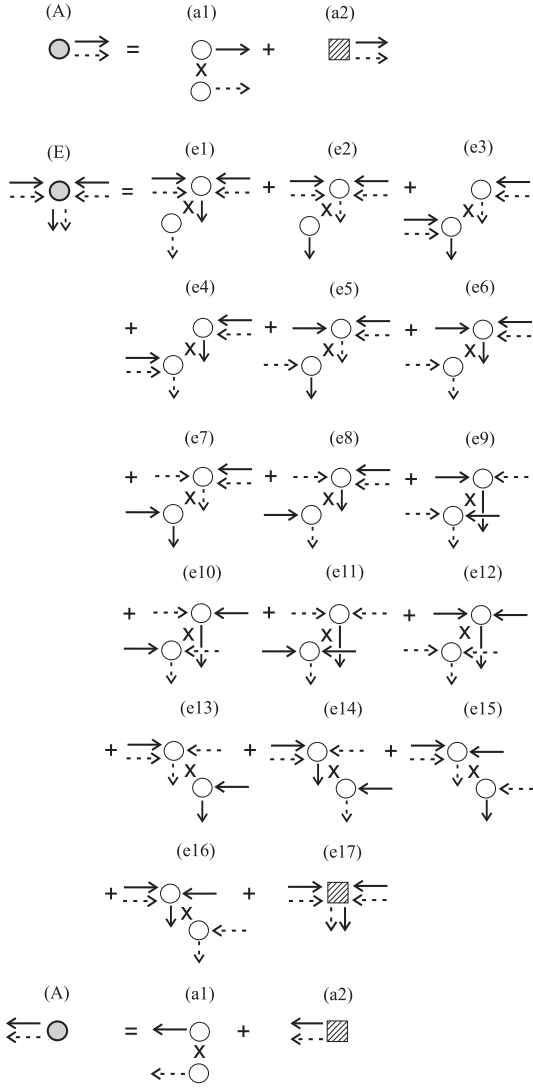


FIG. 8: (Left) single-atom building blocks contributing to the ladder spectrum of type 2; (right) expansion of the single-atom building blocks in elementary single-atom building blocks.

diagrams. Again, the mathematical expressions for the elementary building blocks shown in Fig. 9 (as well as those shown in Fig. 11, see Sec. IV C) are given in Sec. V, see Eqs. (27) and (37).

By combining all diagrams (A), (E), (A), we obtain $68 = 2 \times 17 \times 2$ terms, the sum of which must finally be multiplied by a factor 3 in order to obtain the expression $L_{\text{tot},2}^{(3)}$ for the ladder intensity of type 2, see Eq. (17).

C. Crossed contribution

1. Type 1

Recall that this contribution describes interference between counter-propagating amplitudes. Its graphical rep-

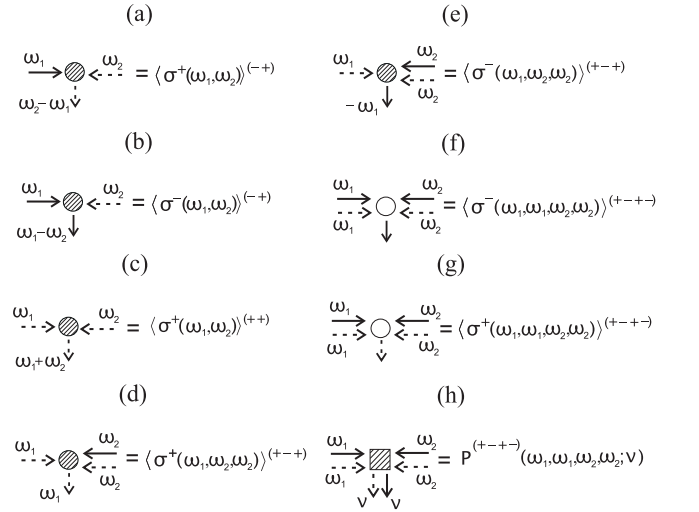


FIG. 9: Elementary building blocks required to describe the response of the intermediate atom in Fig. 8 account for 2, 3, and 4 arrows with frequencies ω_1 and ω_2 . (a)-(g) scattering amplitudes; (h) frequency correlation function.

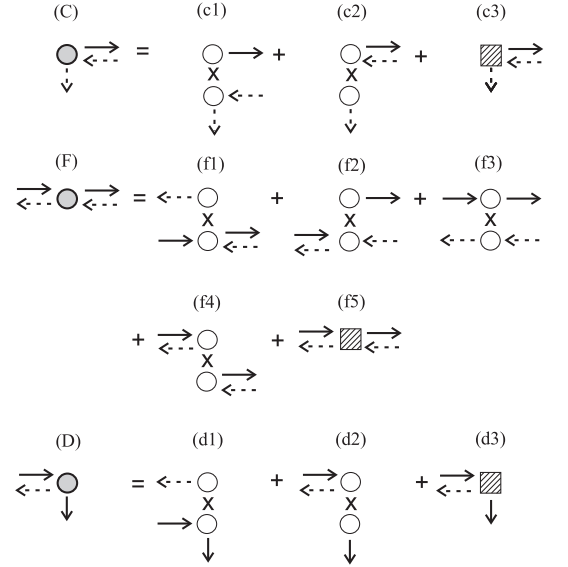


FIG. 10: (Left) single-atom building blocks for the crossed contribution of type 1 arising due to interference between the counter-propagating amplitudes, see Fig. 5(c). The detected signal originates from the blocks (C) and (D); (right) expansion of the right hand side into the elementary single-atom building blocks.

resentation shown in Fig. 10 is constructed analogously to the ladder terms by expanding, on the right hand side, each of the single-atom building blocks (C), (F), and (D) into a sum of elastic and inelastic responses.

The diagrammatic expansion of the block (F), apparently, contains the new response function $P^{(-+)}(\omega_1, \omega_2; \nu)$ shown in Fig. 11(a). However, in full analogy with the functions $\langle \sigma^\pm(\omega_1, \omega_2) \rangle^{(\pm)}$, the function $P^{(-+)}(\omega_1, \omega_2; \nu)$ is the same as the function

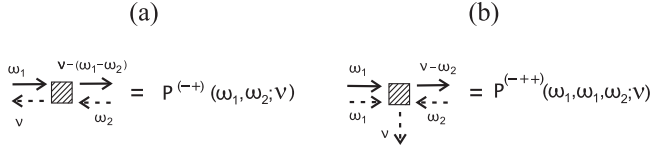


FIG. 11: Elementary building blocks required to describe the inelastic response of the intermediate atom: (a) block (f5) in Fig. 10; (b) block (g9) in Fig. 12.

$P^{(-+)}(\omega, \omega; \nu)$ shown in Fig. 6(h), but taken with different frequency arguments corresponding to the incoming arrows.

Combining all contributions (C), (F), and (D) yields 45 terms. However, 13 of them contain closed loops (see Appendix D), and are forbidden according to the rules of combining diagrams (see Sec. IV D). Only the remaining 32 triple scattering diagrams (multiplied by a factor 6) thus contribute to the crossed intensity $C_{\text{tot},1}^{(3)}$ of type 1, see Eq. (22).

2. Type 2

Expanding the single-atom blocks (A), (G), and (D) into the elastic and inelastic responses, we obtain 2, 9, and 3 diagrams, respectively, in the right hand side of Fig. 12. Analyzing the diagrams contributing to block (G), we notice a new term displayed in Fig. 11(b).

Combining single-atom responses on the right hand side of Fig. 12 yields 56 terms. Excluding the diagrams featuring closed loops (8 diagrams, see Appendix D) we come up with 46 terms. Finally, the crossed intensity $C_{\text{tot},2}^{(3)}$ of type 2 results as 12 times the real part, see Eq. (23), of the sum of all these 46 terms.

D. Self-consistent combination of single-atom building blocks

Figures 7, 8, 10 and 12 present diagrammatic expansions of the single-atom responses in the elementary single-atom building blocks. To obtain the triple scattering ladder and crossed spectra from these expansions, we combine the elementary blocks in a self-consistent way [24].

First, we compose the three-atom diagrams using single-atom blocks by connecting the outgoing arrows with incoming ones regarding the direction and character (solid or dashed) thereof. Second, according to the spectral responses functions associated with the blocks given in Figs. 6, 9, and 11, we ascribe frequency values to each of the inelastic (that is, distinct from the laser frequency) arrows in the resulting diagrams. In doing this, we also keep in mind that the two outgoing (downward) arrows correspond to the spectral intensity of the backscattered light at a given frequency, and must have the same fre-

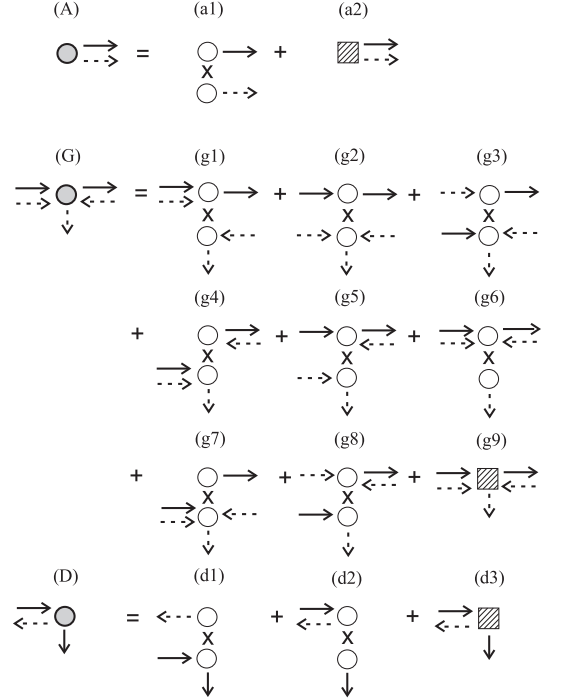


FIG. 12: (Left) single-atom building blocks for the crossed contribution of type 2 arising due to interference between the counter-propagating amplitudes, see Fig. 5(d). The detected signal originates from the blocks (G) and (D); (right) expansion of the right hand side into the elementary single-atom building blocks.

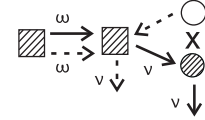


FIG. 13: Example of a triple scattering interference spectral response obtained by self-consistently combining diagrams (a2), (g9), and (d1) from Fig. 12.

quency value ν . Finally, all intermediate inelastic frequencies which alter upon scattering are integrated over.

We already mentioned that 13 diagrams resulting from Fig. 10 and 8 – from Fig. 12 are forbidden because they contain closed loops wherein the scattered amplitudes travel between the atoms without going out (see an example of a loop in Appendix D). We note that similar forbidden diagrams appear also in a nonlinear transport theory of classical scatters [30].

It is instructive to illustrate the above rules by an example. For that, consider a self-consistent combination of diagrams (a2)(g9)(d1) (see Fig. 12), which constitutes 1 of the 46 diagrams contributing to the crossed intensity of type 2. The corresponding compound diagram is drawn in Fig. 13. The symbolic expressions for the response functions corresponding to the elementary building blocks appearing in Fig. 13 are given in Figs. 6(a), (b), (e), and 11(b) (more precisely, the block in Fig. 6(a)

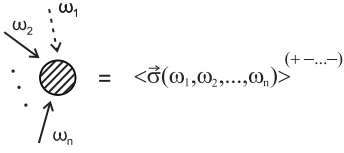


FIG. 14: Circle with incoming dashed and solid arrows at frequencies $\omega_1, \omega_2, \dots, \omega_n$, representing the n th order correction to the optical Bloch vector $\langle \vec{\sigma}(\omega_1, \omega_2, \dots, \omega_n) \rangle^{(+ - \dots -)}$, whose frequencies and signs in the superscript are arranged in the same order. The signs ‘+’ and ‘-’ are associated with dashed and solid arrows, respectively. The positive and negative frequency amplitudes associated with this block have frequency $\sum_i s_i \omega_i$ which is in general non-zero, i.e. detuned from the laser frequency, and hence the circle is hatched.

is the complex conjugate of the one from Fig. 13). Noting that the intermediate inelastic frequency ω changes its value, we obtain the following result for the contribution:

$$(a2)(g9)(d1) = \int_{-\infty}^{\infty} d\omega P^{(0)}(\omega) P^{(-++)}(\omega, \omega, 0; \nu) \times \langle \sigma^+ \rangle^{(0)} \langle \sigma^- \rangle^{(-)}, \quad (24)$$

where we have omitted the prefactor $\langle T_{21}^* T_{32}^* T_{12} T_{32} \rangle_{\text{conf}}$ which scales as $(k_L \ell)^{-4}$ (see Eq. (2)), where ℓ is the mean interatomic distance. Any other combination of the elementary building blocks is expressed in an analogous way. Further examples are considered in Sec. VI.

V. GENERAL EXPRESSIONS FOR SINGLE-ATOM BUILDING BLOCKS

In the previous Secs. III and IV we introduced diagrams for all elementary single atom building blocks, see Figs. 7, 8, 10 and 12, exhibiting at most four incoming arrows. In this section, we will give the corresponding mathematical expressions, generalized to an arbitrary number n of incoming probe fields.

It is important to have formulae for an arbitrary n for the following reasons: First, the laser-driven cold atoms in a cloud experience random polychromatic fields which can be modeled by a large number of the incident arrows labeled by different frequencies [22]. Second, already in case of three incoming arrows the expressions for the building blocks become rather heavy. It is these

two considerations that urged us to look for a general and concise description of the building blocks. Such a formulation is possible due to the clear hierarchical structure of the building blocks and the small number of constituents needed for their construction.

To compose an arbitrary spectral response function, we need (i) the single-atom Green’s function $G(z) = (z - M)^{-1}$, where $M = M_\lambda$ according to Eq. (A2) with $\Omega_\lambda = \Omega$ for an atom placed at the coordinate origin; (ii) the matrices $\Delta^{(+)}$ and $\Delta^{(-)}$ describing the coupling of the negative- and positive-frequency probe fields to the atomic dipole (Eq. (A8)); (iii) frequency values and types (dashed or solid) of all the incoming probe fields.

A. Spectral response functions associated with the Bloch vector

In the hierarchy of the single-atom building blocks, the most basic element is the steady state optical Bloch vector for an atom interacting with a laser field alone. We will represent this vector graphically by a blank circle:

$$\bigcirc = \langle \vec{\sigma} \rangle^{(0)} = G \vec{L}, \quad (25)$$

where \vec{L} is given in Eq. (A2), and $G \equiv G(0)$.

Circles with one, two, ..., n incoming arrows describe perturbative corrections to the Bloch vector due to one, two, ..., n weak classical probe fields. Equivalently, these corrections can be regarded as arising from the excitation transfer processes from the surrounding atoms (see Sec. III C 1). A graphical representation of the n th order correction $\langle \vec{\sigma}(\omega_1, \omega_2, \dots, \omega_n) \rangle^{(+ - \dots -)}$ for a particular choice of the incoming arrows is shown in Fig. 14.

As follows from Fig. 14, we associate signs s_j ($j = 1, \dots, n$) with each of the n incoming arrows according to the rule

$$s_j = \begin{cases} -, & \text{for incoming } \longrightarrow, \\ +, & \text{for incoming } \dashrightarrow. \end{cases} \quad (26)$$

We stress that, to avoid confusion, we always arrange frequencies and the corresponding signs in the same order.

With these preliminary remarks, we introduce the general expression for the vector $\langle \vec{\sigma}(\omega_1, \omega_2, \dots, \omega_n) \rangle^{(s_1 s_2 \dots s_n)}$:

$$\langle \vec{\sigma}(\omega_1, \omega_2, \dots, \omega_n) \rangle^{(s_1 s_2 \dots s_n)} = \sum_{\pi(j_1, \dots, j_n)} G(i \sum_{k=1}^n s_{j_k} \omega_{j_k}) \Delta^{(s_{j_n})} \dots G(i s_{j_1} \omega_{j_1} + i s_{j_2} \omega_{j_2}) \Delta^{(s_{j_2})} G(i s_{j_1} \omega_{j_1}) \Delta^{(s_{j_1})} G \vec{L}, \quad (27)$$

where $\pi(j_1, \dots, j_n)$ denotes $n!$ permutations of indices

$j_1, \dots, j_n \in \{1, \dots, n\}$. As can be proven by the method

of induction, the same expression is obtained when expanding the quasi-stationary solution of the optical Bloch equations for an atom driven by a superposition of the laser field plus n additional fields with different frequencies $\omega_1, \dots, \omega_n$ up to first order in each of the additional field's amplitudes.

To illustrate application of the formula (27) by an example, we will consider the function $\langle \vec{\sigma}(\omega_1, \omega_2) \rangle^{(+)}$ describing a second-order correction to the Bloch vector due to the incoming negative and positive frequency amplitudes at frequencies ω_1 and ω_2 , respectively (Fig. 9(b)). By virtue of Eq. (27) we obtain:

$$\begin{aligned} \langle \vec{\sigma}(\omega_1, \omega_2) \rangle^{(+)} &= G(i[\omega_1 - \omega_2])\Delta^{(-)}G(i\omega_1)\Delta^{(+)}G\vec{L} \\ &+ G(i[\omega_1 - \omega_2])\Delta^{(+)}G(-i\omega_2)\Delta^{(-)}G\vec{L}. \end{aligned} \quad (28)$$

The first and second element of the vector $\langle \vec{\sigma}(\omega_1, \dots, \omega_n) \rangle^{(s_1 \dots s_n)}$, $\langle \sigma^-(\omega_1, \dots, \omega_n) \rangle^{(s_1 \dots s_n)}$ and $\langle \sigma^+(\omega_1, \dots, \omega_n) \rangle^{(s_1 \dots s_n)}$, correspond to the outgoing positive and negative frequency amplitude depicted by a solid and dashed arrow, respectively. The simplest outgoing amplitudes correspond to absent incoming arrows:

$$\bigcirc \longrightarrow = \langle \sigma^- \rangle^{(0)} = [G\vec{L}]_1, \quad (29)$$

$$\bigcirc \dashrightarrow = \langle \sigma^+ \rangle^{(0)} = [G\vec{L}]_2. \quad (30)$$

The frequencies of the outgoing arrows are uniquely defined by those of the incoming ones and are equal to $-\sum_j s_j \omega_j$ for a solid and $+\sum_j s_j \omega_j$ for a dashed arrow. Unless, for each arrow with non-zero detuning ω_j there exists a corresponding complex conjugate arrow with the same detuning, $\sum_j s_j \omega_j \neq 0$. In Fig. 14, we have assumed that the latter is true, and therefore hatched the circle.

B. Spectral response functions associated with correlation functions

Previously, we described the amplitude response functions which are depicted graphically by a circle with

$n \geq 0$ incoming and a single outgoing arrows. Now, we will consider the building blocks with two outgoing arrows, of which one is solid and one dashed. In general, these building blocks are associated with the atomic dipole correlation functions [24]. As already mentioned above, splitting these functions into a factorizable and non-factorizable component then defines the elastic and inelastic component of the radiated intensity.

1. Factorized response functions

In the beginning, we will consider the building blocks which can be factorized as products of the negative and positive frequency scattering amplitudes. In the simplest case of no incoming arrows, such a product gives the intensity of the elastic component of resonance fluorescence. Graphically, this quantity is represented as

$$\begin{aligned} &\bigcirc \dashrightarrow \\ &\times \\ &\bigcirc \longrightarrow. \end{aligned} \quad (31)$$

For an arbitrary number n of the incoming arrows, they can be distributed among the outgoing positive and negative frequency amplitudes of a factorized correlation function in 2^n ways. The resulting correlation function is then expanded into a sum of these 2^n combinations. For $n \leq 3$, the diagrammatic expansions are given in Figs. 7, 10, and 12.

In the following, we will use permutations between the sets of indices $\{j_1, \dots, j_k\}$ and $\{j_{k+1}, \dots, j_n\}$, which we will denote by $\pi(j_1, \dots, j_k | j_{k+1}, \dots, j_n)$. There are $n!/k!(n-k)!$ such permutations. Now, if there are n incoming arrows, the factorized response function $g^{(s_1 \dots s_n)}(\omega_1, \dots, \omega_n)$ reads

$$\begin{aligned} g^{(s_1 \dots s_n)}(\omega_1, \dots, \omega_n) &= \langle \sigma^+(\omega_1, \dots, \omega_n) \rangle^{(s_1 \dots s_n)} \langle \sigma^- \rangle^{(0)} \\ &+ \sum_{\pi(j_1, \dots, j_{n-1} | j_n)} \langle \sigma^+(\omega_{j_1}, \dots, \omega_{j_{n-1}}) \rangle^{(s_{j_1} \dots s_{j_{n-1}})} \langle \sigma^-(\omega_{j_n}) \rangle^{(s_{j_n})} \\ &+ \dots \\ &+ \sum_{\pi(j_1 | j_2, \dots, j_n)} \langle \sigma^+(\omega_{j_1}) \rangle^{(s_{j_1})} \langle \sigma^-(\omega_{j_2}, \dots, \omega_{j_n}) \rangle^{(s_{j_2} \dots s_{j_n})} \\ &+ \langle \sigma^+ \rangle^{(0)} \langle \sigma^-(\omega_1, \dots, \omega_n) \rangle^{(s_1 \dots s_n)}. \end{aligned} \quad (32)$$

Let us illustrate Eq. (32) by an example for $n = 2$:

$$g^{(+ -)}(\omega_1, \omega_2) = \langle \sigma^+(\omega_1, \omega_2) \rangle^{(+ -)} \langle \sigma^- \rangle^{(0)} + \langle \sigma^-(\omega_1, \omega_2) \rangle^{(+ -)} \langle \sigma^+ \rangle^{(0)} \\ + \langle \sigma^+(\omega_1) \rangle^{(+)} \langle \sigma^-(\omega_2) \rangle^{(-)} + \langle \sigma^-(\omega_1) \rangle^{(+)} \langle \sigma^+(\omega_2) \rangle^{(-)}, \quad (33)$$

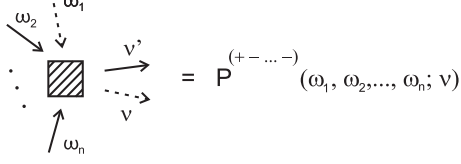


FIG. 15: Inelastic building blocks have two outgoing arrows. The frequencies of the outgoing and incoming arrows are related by the energy conservation relation $\nu - \nu' = \sum_k s_k \omega_k$ (see Eq. (34)).

where the subsequent terms of Eq. (33) correspond to diagrams (f1), (f2), (f3), and (f4) with the frequencies of the incoming dashed and solid arrows equal to ω_1 and ω_2 , respectively (see Fig. 10).

2. Non-factorized response functions

The fluctuating part of the atomic dipole correlation function cannot be factorized. The building blocks associated with such functions are depicted by hatched boxes with one dashed and one solid outgoing arrows (see Fig. 15), and are denoted by $P^{(s_1 \dots s_n)}(\omega_1, \dots, \omega_n; \nu)$. In this case, the frequencies of the outgoing arrows are not defined only by those of the incoming ones: an additional frequency ν appears which describes the spectral distribution of the outgoing, say dashed, arrow. The fre-

quency ν' of the outgoing solid arrow is related to ν by the identity

$$\nu' \equiv \nu - \sum_{k=1}^n s_k \omega_k, \quad (34)$$

which reflects the energy conservation upon the scattering process.

It is well known how to obtain the inelastic part of the emission spectrum of a laser-driven atom (see, for instance, [15]). To find the function $P^{(s_1 \dots s_n)}(\omega_1, \dots, \omega_n; \nu)$, we have generalized the same procedure to account, in addition to the laser field, for the presence of n probe fields.

An important ingredient in the definition of the function $P^{(s_1 \dots s_n)}(\omega_1, \dots, \omega_n; \nu)$ are the expressions for the fluctuating part of the n th order correction of atomic dipole correlation functions. These expressions can be straightforwardly obtained with the aid of the n th-order correction to the Bloch vector $\langle \vec{\sigma}(\omega_1, \dots, \omega_n) \rangle^{(s_1 \dots s_n)}$, Eq. (27), and the factorized response function $g^{(s_1 \dots s_n)}(\omega_1, \dots, \omega_n)$, Eq. (32).

Using the function $g^{(s_1 \dots s_n)}(\omega_1, \dots, \omega_n)$, we create two vector functions, $\vec{g}_+^{(s_1 \dots s_n)}(\omega_1, \dots, \omega_n)$ and $\vec{g}_-^{(s_1 \dots s_n)}(\omega_1, \dots, \omega_n)$. The former and latter vectors are obtained by making substitutions $\sigma^+ \rightarrow \vec{\sigma}$ and $\sigma^- \rightarrow \vec{\sigma}$, respectively, in each of the terms of Eq. (32). Explicitly,

$$\vec{g}_\pm^{(s_1 \dots s_n)}(\omega_1, \dots, \omega_n) = \langle \vec{\sigma}(\omega_1, \dots, \omega_n) \rangle^{(s_1 \dots s_n)} \langle \sigma^\mp \rangle^{(0)} \\ + \sum_{\pi(j_1, \dots, j_{n-1} | j_n)} \langle \vec{\sigma}(\omega_{j_1}, \dots, \omega_{j_{n-1}}) \rangle^{(s_{j_1} \dots s_{j_{n-1}})} \langle \sigma^\mp(\omega_{j_n}) \rangle^{(s_{j_n})} \\ + \dots \\ + \sum_{\pi(j_1 | j_2, \dots, j_n)} \langle \vec{\sigma}(\omega_{j_1}) \rangle^{(s_{j_1})} \langle \sigma^\mp(\omega_{j_2}, \dots, \omega_{j_n}) \rangle^{(s_{j_2} \dots s_{j_n})} \\ + \langle \vec{\sigma} \rangle^{(0)} \langle \sigma^\mp(\omega_1, \dots, \omega_n) \rangle^{(s_1 \dots s_n)}. \quad (35)$$

Now, the fluctuating part of the atomic dipole correlation function reads:

$$\vec{q}_\pm^{(s_1 \dots s_n)}(\omega_1, \dots, \omega_n) = \mp i \Delta^{(\pm)} \langle \vec{\sigma}(\omega_1, \dots, \omega_n) \rangle^{(s_1 \dots s_n)} - \vec{g}_\pm^{(s_1 \dots s_n)}(\omega_1, \dots, \omega_n). \quad (36)$$

In case of no incoming arrows, Eq. (36) reduces to the

following expressions:

$$\vec{q}_+^{(0)} = -i \Delta^{(+)} \langle \vec{\sigma} \rangle^{(0)} + \vec{L}_1 - \langle \vec{\sigma} \rangle^{(0)} \langle \sigma^- \rangle^{(0)}, \\ \vec{q}_-^{(0)} = i \Delta^{(-)} \langle \vec{\sigma} \rangle^{(0)} + \vec{L}_2 - \langle \vec{\sigma} \rangle^{(0)} \langle \sigma^+ \rangle^{(0)},$$

where the $\vec{L}_1 = (0, 1/2, 0)^T$, and $\vec{L}_2 = (1/2, 0, 0)^T$ appear due to the identity $\langle \sigma^+ \sigma^- \rangle^{(0)} \equiv (1 + \langle \sigma^z \rangle^{(0)})/2$.

Vectors $\vec{q}_\pm^{(s_1 \dots s_k)}(\omega_1, \dots, \omega_k)$ ($k = 0, 1, \dots, n$) enter the

definition of the inelastic building block shown in Fig. 15 through the relations:

$$P^{(s_1 \dots s_n)}(\omega_1, \dots, \omega_n; \nu) = \frac{1}{2\pi} \left(P_+^{(s_1 \dots s_n)}(\omega_1, \dots, \omega_n; \nu) + P_-^{(s_1 \dots s_n)}(\omega_1, \dots, \omega_n; \nu) \right), \quad (37)$$

where

$$\begin{aligned} P_+^{(s_1 \dots s_n)}(\omega_1, \dots, \omega_n; \nu) &= \sum_{\pi(j_1, \dots, j_n)} \left[G(i\nu) \Delta^{(s_{j_n})} \dots \Delta^{(s_{j_2})} G(i\nu' + i s_{j_1} \omega_{j_1}) \Delta^{(s_{j_1})} G(i\nu') \vec{q}_+^{(0)} \right]_2 \\ &+ \sum_{\pi(j_2, \dots, j_n)} \left[G(i\nu) \Delta^{(s_{j_n})} \dots \Delta^{(s_{j_2})} G(i\nu' + i s_{j_1} \omega_{j_1}) \vec{q}_+^{(s_{j_1})}(\omega_{j_1}) \right]_2 \\ &+ \dots \\ &+ \left[G(i\nu) \vec{q}_+^{(s_{j_1} \dots s_{j_n})}(\omega_{j_1}, \dots, \omega_{j_n}) \right]_2, \end{aligned} \quad (38a)$$

$$\begin{aligned} P_-^{(s_1 \dots s_n)}(\omega_1, \dots, \omega_n; \nu) &= \sum_{\pi(j_1, \dots, j_n)} \left[G(-i\nu') \Delta^{(s_{j_n})} \dots \Delta^{(s_{j_2})} G(-i\nu + i s_{j_1} \omega_{j_1}) \Delta^{(s_{j_1})} G(-i\nu) \vec{q}_-^{(0)} \right]_1 \\ &+ \sum_{\pi(j_2, \dots, j_n)} \left[G(-i\nu') \Delta^{(s_{j_n})} \dots \Delta^{(s_{j_2})} G(-i\nu + i s_{j_1} \omega_{j_1}) \vec{q}_-^{(s_{j_1})}(\omega_{j_1}) \right]_1 \\ &+ \dots \\ &+ \left[G(-i\nu') \vec{q}_-^{(s_{j_1} \dots s_{j_n})}(\omega_{j_1}, \dots, \omega_{j_n}) \right]_1, \end{aligned} \quad (38b)$$

with ν' defined in Eq. (34). Again, as can be proven by the method of induction, Eqs. (37-38) coincide with the expressions obtained from the perturbative solution for a single atom driven by a laser field and additional weak probe fields.

Finally, we will illustrate Eqs. (37), (38) by the simplest non-trivial example of the expression for a hatched box with one incoming dashed arrow at frequency ω (see, e.g., Fig. 10(c3)). In this case we have

$$\begin{aligned} P^{(+)}(\omega; \nu) &= \frac{1}{2\pi} \left(\left[G(i\nu) \Delta^{(+)} G(i\nu - i\omega) \vec{q}_+^{(0)} \right]_2 \right. \\ &+ \left[G(i\nu) \vec{q}_+^{(+)}(\omega) \right]_2 \\ &+ \left[G(i\omega - i\nu) \Delta^{(+)} G(-i\nu) \vec{q}_-^{(0)} \right]_1 \\ &\left. + \left[G(i\omega - i\nu) \vec{q}_-^{(+)}(\omega) \right]_1 \right). \end{aligned} \quad (39)$$

C. Derivation from the master equation

Having defined the elementary single-atom building blocks in Secs. V A and V B, and the rules for connecting them with each other in Sec. IV, we are now able to calculate all the various components (ladder and crossed of type 1 and 2) of the triple scattering intensity in terms of

single-atom quantities. It remains to be shown that the corresponding expressions are identical to those derived from the master equation introduced in Sec. III.

To obtain the solution of the master equation in the form of self-consistent combination of single-atom building blocks, we generalize the method that was previously applied to two atoms [23]. Some steps towards such a solution have been already made in Sec. III. Namely, in Sec. III B we introduced the recurrence relations for vectors $\vec{x}^{(n)}$, $\vec{y}^{(n)}$, and $\vec{z}^{(n)}$. Thereafter, in Sec. III C, we selected the triple scattering diagrams for which the incoherent and interference intensities survive the disorder average, resulting in the ladder and crossed contributions.

The next step is to factorize all terms containing the relevant vectors $\vec{x}^{(4)}$, $\vec{y}^{(4)}$ as combinations of three single-atom expressions. Recall that these vectors include four interaction matrices sandwiched between the Green's functions G_+ , G_\times , or D_\times (see Eq. (12)). The factorization is then accomplished by using the integral representations for G_\times and D_\times which express the two- and three-atom evolution matrices as frequency integrals over tensor products of the single-atom Green's matrices (see Appendix B).

After this procedure, each term contributing to the ladder and crossed intensity contains multiple (up to seven-fold) frequency integrals. Although each integrand repre-

sents a product of three single-atom expressions, neither of them can be interpreted physically. To obtain the physically meaningful single-atom building blocks as defined by the solution of the optical Bloch equations for a single atom, we simplify these expressions further.

To this end, by using the sum rules (see Appendix C) we solve exactly some of the frequency integrals. As a result, we obtain the final expressions for the ladder and crossed spectra which include at most two integrations (see, e.g., Eq. (46) valid for very strong driving $\Omega \gg \gamma$). The ladder spectrum (Fig. 5(a) and (b)) is given by a sum of $118 = 50 + 68$ terms corresponding to all possible combinations of the single-atom building blocks shown in Fig. 7 ($50 = 2 \times 5 \times 5$) and Fig. 8 ($68 = 2 \times 17 \times 2$), see Sec. IV B 1 above. Likewise, the crossed spectrum (Fig. 5(c),(d)) is given by all allowed combinations of the single-atom building blocks shown in Figs. 10 and 12, see Sec. IV C. This completes the derivation of the triple scattering contribution expressed in terms of single-atom response functions.

VI. TRIPLE SCATTERING SPECTRA

In this section, we present our results for the triple scattering spectra of CBS. In the beginning, we provide analytical expressions for the elastic and inelastic contributions in the limit of small Rabi frequency $\Omega \ll \gamma$. Thereafter, we consider the non-perturbative regime of strong atom-laser interaction.

A. Case of small Rabi frequencies ($\Omega \ll \gamma$)

In this limit, it is natural to restrict ourselves to the triple scattering contributions that are not larger than $\sim (\Omega/\gamma)^4$. Physically, this corresponds to a weakly inelastic scattering by three atoms of the laser field containing not more than two photons.

Analyzing the behavior of the triple scattering diagrams, we established that they exhibit different asymptotics when $\Omega \ll \gamma$. For example, the crossed diagram (a2)(g9)(d1) (see Eq. (24)) yields an expression which is $\sim (\Omega/\gamma)^6$, and can therefore be neglected. We will consider separately the elastic and inelastic components of CBS.

1. Elastic spectrum

Diagrams in Fig. 16(a)-(e) describe the elastic ladder intensity $L_{el,1}^{(3)}$. They can be presented in the form of equations: (a)=(a1)(b3)(b3), (b)=(a1)(b3)(b2), (c)=(a1)(b3)(b1), (d)=(a1)(b1)(b3), and (e)=(a1)(b2)(b3), where the compounds on the right hand sides are the single-atom building blocks from Fig. 7. Figure 17(a-d) depicts diagrams contribut-

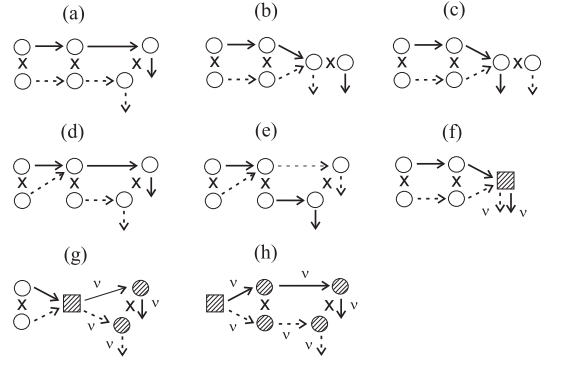


FIG. 16: Triple scattering diagrams yielding the elastic (a-e) and inelastic (f-h) ladder spectra of type 1. For one-photon processes ($\sim \Omega^2$), only diagram (a) contributes.

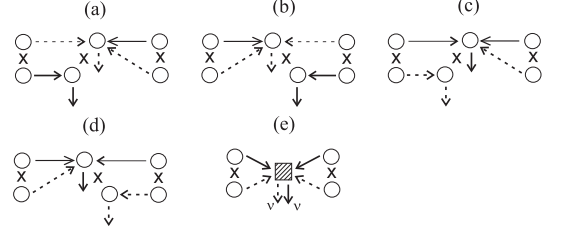


FIG. 17: Triple scattering diagrams yielding the elastic (a-d) and inelastic (e) ladder spectra of type 2.

ing to $L_{el,2}^{(3)}$. In this case, the corresponding equations for diagrams read (see Fig. 8): (a)=(a1)(e7)(a1), (b)=(a1)(e13)(a1), (c)=(a1)(e6)(a1), (d)=(a1)(e16)(a1).

Likewise, the elastic crossed contributions in Fig. 18(a)-(e) result from the combinations of single-atom blocks of Fig. 10: (a)=(c1)(f3)(d1), (b)=(c1)(f1)(d1), (c)=(c1)(f2)(d1), (d)=(c2)(f3)(d1), (e)=(c1)(f3)(d2), which yield the elastic crossed intensity $C_{el,1}^{(3)}$. Finally, the four diagrams in Fig. 19 yield the crossed contribution $C_{el,2}^{(3)}$. They are composed of the diagrams of

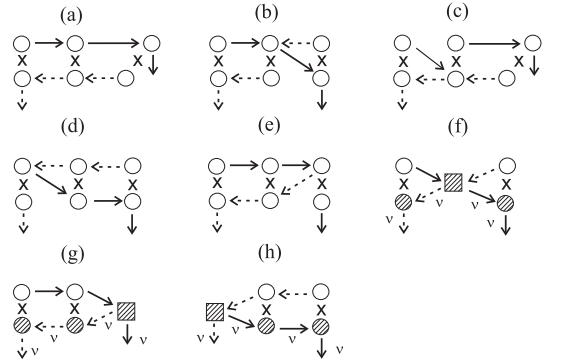


FIG. 18: Triple scattering diagrams yielding the elastic (a-e) and inelastic (f-h) crossed spectra of type 1. For one-photon processes, only diagram (a) which is a reciprocal of diagram (a) in Fig. 16, contributes.

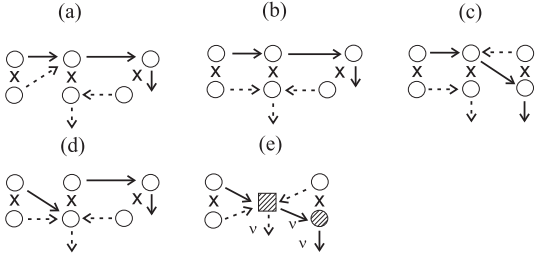


FIG. 19: Triple scattering diagrams yielding the elastic (a-d) and inelastic (e) crossed spectra of type 2.

Fig. 12 as follows: (a)=(a1)(g1)(d1), (b)=(a1)(g2)(d1), (c)=(a1)(g5)(d1), (d)=(a1)(g7)(d1).

We obtain the following analytical expressions for the elastic triple scattering ladder and crossed intensities which are valid up to $(\Omega/\gamma)^4$:

$$L_{el,1}^{(3)} = \frac{3\tilde{\Omega}^2}{32(1+\tilde{\delta}^2)^3} - \frac{27\tilde{\Omega}^4}{32(1+\tilde{\delta}^2)^4}, \quad (40a)$$

$$L_{el,2}^{(3)} = -\frac{6\tilde{\Omega}^4}{32(1+\tilde{\delta}^2)^4}, \quad (40b)$$

$$C_{el,1}^{(3)} = \frac{3\tilde{\Omega}^2}{32(1+\tilde{\delta}^2)^3} - \frac{24\tilde{\Omega}^4}{32(1+\tilde{\delta}^2)^4}, \quad (40c)$$

$$C_{el,2}^{(3)} = -\frac{24\tilde{\Omega}^4}{32(1+\tilde{\delta}^2)^4}, \quad (40d)$$

where $\tilde{\Omega} = \Omega/\gamma$, $\tilde{\delta} = \delta/\gamma$. Using the above results, which, as we have checked, coincide with the results following from the two-photon scattering theory [13], we draw two conclusions. First, in the linear regime, only the diagrams in Figs. 16(a) and 18(a) contribute to the signal, and ladder and crossed components are equal to each other, what indicates perfect phase coherence in the linear regime. From Eqs. (40a) and (40c) it follows that

$$L_{el,1}^{(3)} = C_{el,1}^{(3)} = \frac{3\tilde{\Omega}^2}{32(1+\tilde{\delta}^2)^3}. \quad (41)$$

Second, at increased Rabi frequencies, the interference contribution $C_{el,1}^{(3)} + C_{el,2}^{(3)}$ decreases faster than the ladder contribution $L_{el,1}^{(3)} + L_{el,2}^{(3)}$, since the contributions proportional to $\tilde{\Omega}^4$ have a negative sign, and are larger for the crossed component ($24 + 24 = 48$) than for the ladder component ($27 + 6 = 33$), see Eqs. (40). The fact that the interference contribution exceeds the background can be explained by the fact that, in the case of nonlinear triple scattering, the coherent backscattering signal is in general formed by *three* interfering amplitudes [13].

2. Inelastic spectrum

The four inelastic ladder diagrams are depicted in Fig. 16(f)-(h) and Fig. 17(e). These diagrams result from

the combinations: (f)=(a1)(b3)(b5), (g)=(a1)(b5)(b3), (h)=(a2)(b3)(b3) (see Fig. 7), (e)=(a1)(e17)(a1) (see Fig. 8).

Concerning the inelastic crossed spectrum, it is given by the four contributions shown in Fig. 18(f)-(h) and Fig. 19(e). Diagrams (f)-(h) consist of the following building blocks: (f)=(c1)(f5)(d1), (g)=(c1)(f3)(d3), and (h)=(c3)(f3)(d1), with the right hand sides coming from Fig. 10. ‘‘Type 2’’ crossed diagram in Fig. 19(e) yields one contribution to the inelastic spectrum in the weakly inelastic regime: (e)=(a1)(g9)(d1), with the constituents defined in Fig. 12. Due to this contribution which emerges when the scatterers are nonlinear [13, 30], the interference effect modifies dramatically: the enhancement factor associated with the inelastic scattering becomes greater than 2, again due to the interference between three amplitudes mentioned above.

Indeed, consider the analytical expressions for the inelastic ladder and crossed spectra:

$$L_{inel,1}^{(3)}(\tilde{\nu}) = \frac{1}{2\pi} \frac{6\tilde{\Omega}^4}{32(1+\tilde{\delta}^2)^3} \quad (42a)$$

$$\times \frac{(3(1+\tilde{\delta}^2) + 4\tilde{\delta}\tilde{\nu} + 2\tilde{\nu}^2)^2}{(1+(\tilde{\delta}-\tilde{\nu})^2)(1+(\tilde{\delta}+\tilde{\nu})^2)^3},$$

$$L_{inel,2}^{(3)}(\tilde{\nu}) = \frac{1}{2\pi} \frac{\tilde{\Omega}^4}{32(1+\tilde{\delta}^2)^3} \quad (42b)$$

$$\times \frac{12}{(1+(\tilde{\delta}-\tilde{\nu})^2)(1+(\tilde{\delta}+\tilde{\nu})^2)}$$

$$C_{inel,1}^{(3)}(\tilde{\nu}) = \frac{1}{2\pi} \frac{6\tilde{\Omega}^4}{4(1+\tilde{\delta}^2)^3} \quad (42c)$$

$$\times \frac{(1+\tilde{\delta}(\tilde{\delta}+\tilde{\nu}))^2}{(1+(\tilde{\delta}-\tilde{\nu})^2)(1+(\tilde{\delta}+\tilde{\nu})^2)^3},$$

$$C_{inel,2}^{(3)}(\tilde{\nu}) = \frac{1}{2\pi} \frac{6\tilde{\Omega}^4}{4(1+\tilde{\delta}^2)^3} \quad (42d)$$

$$\times \frac{1+\tilde{\delta}(\tilde{\delta}+\tilde{\nu})}{(1+(\tilde{\delta}-\tilde{\nu})^2)(1+(\tilde{\delta}+\tilde{\nu})^2)^2}.$$

As we have checked, the inelastic spectra given by Eqs. (42) are also in full agreement with the two-photon diagrammatic scattering theory [13]. The curves corresponding to the functions $L_{inel}^{(3)}(\nu) = L_{inel,1}^{(3)}(\nu) + L_{inel,2}^{(3)}(\nu)$ and $C_{inel}^{(3)}(\nu) = C_{inel,1}^{(3)}(\nu) + C_{inel,2}^{(3)}(\nu)$, are plotted in Fig. 20.

It is clearly seen that the dashed line corresponding to $C_{inel}^{(3)}(\nu)$ is above the solid line corresponding to $L_{inel}^{(3)}(\nu)$. To characterize this effect in more quantitative terms, let us, following [13], assume that the elastic component has been filtered out, and study the behavior of the enhancement factor, which in this case is defined as

$$\eta = 1 + \frac{C_{inel}^{(3)}}{L_{inel}^{(3)}}. \quad (43)$$

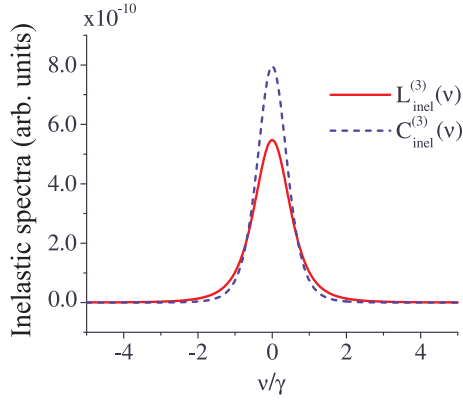


FIG. 20: (Color online) Inelastic ladder and crossed spectra of triple scattering for the case of exact resonance ($\delta = 0$) and $\Omega = 0.01\gamma$.

Integrating Eqs. (42) over $\tilde{\nu}$, we obtain:

$$C_{\text{inel}}^{(3)} = \frac{3(22 + \tilde{\delta}^2)\tilde{\Omega}^4}{128(1 + \tilde{\delta}^2)^4}, \quad (44)$$

$$L_{\text{inel}}^{(3)} = \frac{3(154 + 25\tilde{\delta}^2 + 3\tilde{\delta}^4)\tilde{\Omega}^4}{1024(1 + \tilde{\delta}^2)^4}, \quad (45)$$

wherefrom we deduce that $\eta(\tilde{\delta}) > 2$ for $|\tilde{\delta}| < 1.042$, with the maximum value of ≈ 2.143 at $\tilde{\delta} = 0$. In fact, in a cloud consisting of a large number of atoms, and applying appropriate frequency filtering, the enhancement factor (43) can in principle reach the value 3 [27].

So far, we have restricted our consideration to the case of weakly inelastic scattering which is valid for very small Rabi frequencies. We will next address the behavior of the CBS spectra in the non-perturbative regime of the atom-light interaction.

B. Non-perturbative account of atom-laser interaction

If the Rabi frequency does not satisfy the condition $\Omega \ll \gamma$, we enter the regime of light scattering by atoms wherein the non-perturbative expressions for the single-atom building blocks must be used. Consequently, we consider contributions from all triple scattering diagrams resulting from self-consistent combinations of the single-atom building blocks shown in Figs. 7, 8, 10, and 12. The results of our numerical calculations of the triple scattering elastic and inelastic spectra are presented in Figs. 21 and 22, respectively.

1. Elastic spectrum

The elastic intensity exhibits an oscillatory-like behavior as a function of the Rabi frequency for $\Omega \lesssim 2\gamma$. The

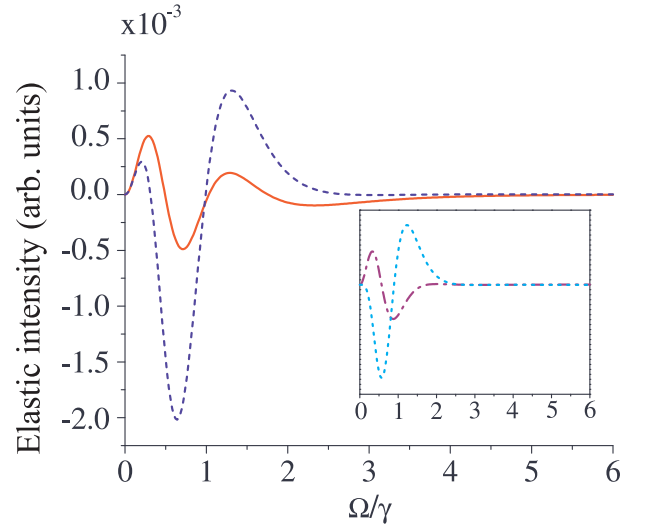


FIG. 21: (Color online) Elastic intensities as a function of Rabi frequency at exact resonance: (solid) $L_{\text{el}}^{(3)}$, (dashed) $C_{\text{el}}^{(3)}$. Inset displays two elastic crossed contributions: (dashed-dotted) $C_{\text{el},1}^{(3)}$; (dotted) $C_{\text{el},2}^{(3)}$.

intensity can assume negative values, which is in accordance with the fact that the triple scattering is observed from the laser-driven transition. Therefore, it is only a correction to the physical intensity which also includes single scattering, and is always positive.

A curious feature exhibited by the crossed contributions in Fig. 21(inset) is that, in a range of Rabi frequencies where the elastic intensity is significant, they have opposite phases. For values of $\Omega \lesssim 0.5\gamma$, $C_{\text{el},2}^{(3)} < 0 < C_{\text{el},1}^{(3)}$. If $0.5\gamma \lesssim \Omega \lesssim \gamma$, both crossed contributions feature destructive interference. In the range $\gamma \lesssim \Omega \lesssim 2\gamma$ the crossed contributions again exhibit opposite interference character: $C_{\text{el},1}^{(3)} < 0 < C_{\text{el},2}^{(3)}$.

Although we have not found a simple explanation of why the two crossed contributions exhibit opposite interference character, this fact is not surprising given that they originate from different triple scattering paths.

2. Inelastic spectrum

To see how inelastic processes affect CBS from three atoms, in Fig. 22 we plot the ladder and crossed spectra for different values of the Rabi frequency. For $\Omega = 0.1\gamma$, the two-photon processes still give the dominant contribution to triple scattering, which is manifest in a qualitative agreement between the spectra in Figs. 22(a) and 20. However, at increased values of the Rabi frequency, Fig. 22(b-f), the crossed spectra are dominated by the ladder spectra. Furthermore, small in magnitude interference spectra feature destructive interference, or CBS anti-enhancement (see Fig. 22(c-f)), due to the crossed contribution of type 2 (see insets).

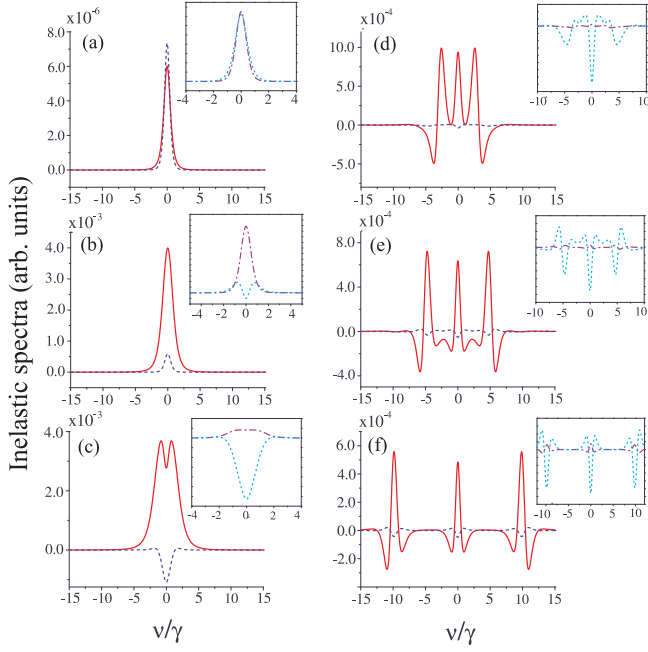


FIG. 22: (Color online) Inelastic ladder (solid) and crossed (dashed) spectra of triple scattering for the case of exact resonance ($\delta = 0$) for different Rabi frequencies: $\Omega =$ (a) 0.1γ ; (b) 0.5γ ; (c) γ ; (d) 3γ ; (e) 5γ ; (f) 10γ . Insets show two inelastic crossed contributions $C_{\text{inel},1}^{(3)}(\tilde{\nu})$ (dashed-dotted) and $C_{\text{inel},2}^{(3)}(\tilde{\nu})$ (dotted).

Increasing the Rabi frequency is also accompanied by a splitting of the ladder and crossed spectra into several Lorentzian and dispersive resonances. This transformation of the spectra can be attributed to the dressing of atomic states by the laser field [20].

For very strong driving strengths $\Omega \gg \gamma$, the intensities of the elastic components become vanishingly small, and the total spectral line shapes are given by the corresponding inelastic spectra. The latter can be deduced by combining the three elementary inelastic building blocks (hatched boxes) for each of the contributions. Namely, the combinations (a2)(b5)(b5), (a2)(e17)(a2), (c3)(f5)(d3), and (a2)(g9)(d3) yield $L_{\text{inel},1}^{(3)}(\nu)$, $L_{\text{inel},2}^{(3)}(\nu)$, $C_{\text{inel},1}^{(3)}(\nu)$, and $C_{\text{inel},2}^{(3)}(\nu)$, respectively (see Figs. 7, 8, 10, and 12). The inelastic ladder and crossed spectra can

then be presented by the compact formulas:

$$L_{\text{inel},1}^{(3)}(\nu) = 6 \int d\omega' d\omega'' P^{(0)}(\omega') \times P^{(+)}(\omega', \omega'; \omega'') P^{(+)}(\omega'', \omega''; \nu), \quad (46a)$$

$$L_{\text{inel},2}^{(3)}(\nu) = 3 \int d\omega' d\omega'' P^{(0)}(\omega') P^{(0)}(\omega'') \times P^{(+--+)}(\omega', \omega', \omega'', \omega''; \nu), \quad (46b)$$

$$C_{\text{inel},1}^{(3)}(\nu) = 6 \int d\omega' d\omega'' P^{(+)}(\omega'; \nu) P^{(-)}(\omega''; \nu) \times P^{(+)}(\nu - \omega'', \nu - \omega'; \omega'), \quad (46c)$$

$$C_{\text{inel},2}^{(3)}(\nu) = 12 \text{Re} \int d\omega' d\omega'' P^{(0)}(\omega') P^{(-)}(\omega''; \nu) \times P^{(+--+)}(\omega', \omega', \nu - \omega''; \nu). \quad (46d)$$

VII. DISCUSSION AND CONCLUSION

We have studied the coherent backscattering of intense laser light from three two-level atoms using the master equation approach. The goal of this work was to find the analytical solution of the problem and show its equivalence with the solution following from the diagrammatic pump-probe approach to CBS. We have fulfilled this task in the spirit of the earlier work [23], where technical tools such as the recurrence relations, the integral representations and spectral decompositions of the Green's matrices, as well as the sum rules were developed and applied to prove the equivalence between the master equation and the pump-probe approaches for double scattering. Here, we have generalized these techniques for three atoms.

From the rigorous analytical solution of the master equation in quadratures, we have found the explicit analytical formulas for the single-atom building blocks whose diagrammatic self-consistent combination yields the triple scattering ladder and crossed spectral intensities. The obtained expressions for the single-atom spectral response functions are equivalent to the pump-probe solutions following from the optical Bloch equations under classical bi- and trichromatic driving fields.

In contrast to double scattering, triple scattering features two crossed contributions in the inelastic scattering regime which manifest the multi-wave character of CBS [30]. It is the interplay between these two contributions that defines the behavior of the overall interference effect as a function of the Rabi frequency. In the weakly inelastic scattering regime, the two inelastic crossed contributions are positive and in phase, yielding the CBS enhancement factor > 2 – in qualitative agreement with the earlier prediction for nonlinear classical scatterers [13]. However, increasing the laser intensity leads to a rapid decrease of the relative intensities of the crossed contributions with respect to the ladder term, on the one hand, and to the destructive interference, on the other hand.

The results of this work go beyond the problem of triple scattering. We have deduced general analytical

expressions for single-atom building blocks for an arbitrary number of incoming probe fields. This corresponds to the case of multiple scattering of intense laser light in a cloud consisting of a large number of atoms, where each atom is radiated both by the coherent laser field and by the fields radiated from all other atoms, the sum of which is not necessarily small compared to the laser field. These expressions can therefore be incorporated into the stochastic pump-probe approach [21, 22] for an accurate simulation of the multiple inelastic scattering of laser light in cold atomic ensembles, including propagation effects in the effective medium, such as the attenuation of the laser field.

Another direction of future work will be to generalize our present results for realistic atoms probed in the CBS ‘‘saturation’’ experiments [5, 6]. This can be achieved by including the polarization degree of freedom into the description of the single-atom response functions.

Acknowledgments

Enjoyable discussions with Sybille Braungardt and Andreas Ketterer are gratefully acknowledged. This work was financially supported by DFG through grant BU-1337/9-1.

Appendix A: Evolution matrices

1. Matrix A : evolution of independent atoms

The blocks of matrix A (see Eq. (11)) read

$$M_+ = M_3 \oplus M_2 \oplus M_1, \quad (\text{A1a})$$

$$M_\times = (M_2 \otimes \mathbb{1} + \mathbb{1} \otimes M_3) \oplus (M_1 \otimes \mathbb{1} + \mathbb{1} \otimes M_3) \oplus (M_1 \otimes \mathbb{1} + \mathbb{1} \otimes M_2), \quad (\text{A1b})$$

$$L_+ = \begin{pmatrix} \vec{L} \otimes \mathbb{1} & \mathbb{1} \otimes \vec{L} & 0 \\ \vec{L} \otimes \mathbb{1} & 0 & \mathbb{1} \otimes \vec{L} \\ 0 & \vec{L} \otimes \mathbb{1} & \mathbb{1} \otimes \vec{L} \end{pmatrix}, \quad (\text{A1c})$$

$$L_\times = (\vec{L} \otimes \mathbb{1} \otimes \mathbb{1} \oplus \mathbb{1} \otimes \vec{L} \otimes \mathbb{1} \oplus \mathbb{1} \otimes \mathbb{1} \otimes \vec{L}), \quad (\text{A1d})$$

$$N_\times = \mathbb{1} \otimes \mathbb{1} \otimes M_3 + \mathbb{1} \otimes M_2 \otimes \mathbb{1} + M_1 \otimes \mathbb{1} \otimes \mathbb{1}. \quad (\text{A1e})$$

Here, $\mathbb{1}$ denotes the unit 3×3 matrix, M_λ ($\lambda = 1, 2, 3$) is a position-dependent 3×3 matrix describing the evolution of the Bloch vector of atom λ , and \vec{L} is a three dimensional vector [23]. Explicitly,

$$M_\lambda = \begin{pmatrix} -\gamma + i\delta & 0 & -i\Omega_\lambda/2 \\ 0 & -\gamma - i\delta & i\Omega_\lambda^*/2 \\ -i\Omega_\lambda^* & i\Omega_\lambda & -2\gamma \end{pmatrix}, \quad \vec{L} = (0, 0, -2\gamma)^T. \quad (\text{A2})$$

To be self-contained, we remind here the form of the optical Bloch equation:

$$\langle \dot{\vec{\sigma}}_\lambda \rangle = M_\lambda \langle \vec{\sigma}_\lambda \rangle + \vec{L}. \quad (\text{A3})$$

Given the vector \vec{L} , we can also define the vector $\vec{\Lambda}$ (see Eq. (9)):

$$\vec{\Lambda} = (\vec{L}, \vec{L}, \vec{L}, \vec{0})^T, \quad (\text{A4})$$

where the null vector in (A4) contains 54 zeroes.

Using Eqs.(A1a) and (14) we obtain

$$G_+(z) = G_3(z) \oplus G_2(z) \oplus G_1(z), \quad (\text{A5})$$

with $G_\lambda(z) = (z - M_\lambda)^{-1}$, cf. Eq. (14)

2. Matrix V : evolution of the dipole-dipole interacting atoms

A convenient way to specify the blocks $(U_{\lambda\mu})_\alpha$, $(W_{\lambda\mu})_\alpha$ ($\alpha = \uparrow, \downarrow, \times$) of the matrix V , see Eqs. (11) and (15), is implicit – by describing their action on test vectors. This is how it was done in the case of two atoms [23]. In fact, due to the pairwise nature of the dipole-dipole interaction, the results for two atoms can, after some modifications, be adapted to the N -atom case. Here, we will sketch this procedure for three atoms.

To this end, we will for the moment abstract ourselves from the presence of a third atom, and consider how the blocks of the ‘contracted’ dipole-dipole interaction matrix (denoted as \bar{v}) act in the two-atom case. When this is done, it is straightforward to define the action of the blocks of the matrix V .

Let \vec{a}_λ and \vec{a}_μ be 3-component column vectors, with the indices λ, μ referring to the atom’s number. Assuming $\lambda < \mu$, we create two test vectors

$$(\vec{p}_{\lambda\mu})_1 = (\vec{a}_\mu, \vec{a}_\lambda)^T, \quad (\vec{p}_{\lambda\mu})_2 = \vec{a}_\lambda \otimes \vec{a}_\mu. \quad (\text{A6})$$

The ‘contracted’ interaction matrices \bar{v}_α ($\alpha = \uparrow, \downarrow, \times$)

are characterized by the following identities [23]:

$$(\bar{v}_{\lambda\mu})_{\lrcorner}(\vec{a}_{\lambda} \otimes \vec{a}_{\mu}) = \begin{pmatrix} 2iT_{\lambda\mu}\Delta^{(+)}\vec{a}_{\mu}[\vec{a}_{\lambda}]_2 \\ \vec{0} \end{pmatrix}, \quad (\text{A7a})$$

$$(\bar{v}_{\mu\lambda})_{\lrcorner}(\vec{a}_{\lambda} \otimes \vec{a}_{\mu}) = \begin{pmatrix} \vec{0} \\ 2iT_{\mu\lambda}\Delta^{(+)}\vec{a}_{\lambda}[\vec{a}_{\mu}]_2 \end{pmatrix}, \quad (\text{A7b})$$

$$(\bar{v}_{\lambda\mu}^*)_{\lrcorner}(\vec{a}_{\lambda} \otimes \vec{a}_{\mu}) = \begin{pmatrix} \vec{0} \\ -2iT_{\lambda\mu}^*\Delta^{(-)}\vec{a}_{\lambda}[\vec{a}_{\mu}]_1 \end{pmatrix}, \quad (\text{A7c})$$

$$(\bar{v}_{\mu\lambda}^*)_{\lrcorner}(\vec{a}_{\lambda} \otimes \vec{a}_{\mu}) = \begin{pmatrix} -2iT_{\mu\lambda}^*\Delta^{(-)}\vec{a}_{\mu}[\vec{a}_{\lambda}]_1 \\ \vec{0} \end{pmatrix}, \quad (\text{A7d})$$

$$(\bar{v}_{\lambda\mu})_{\times}(\vec{a}_{\lambda} \otimes \vec{a}_{\mu}) = -2T_{\lambda\mu}\Delta^{(-)}\vec{a}_{\lambda} \otimes \Delta^{(+)}\vec{a}_{\mu}, \quad (\text{A7e})$$

$$(\bar{v}_{\mu\lambda})_{\times}(\vec{a}_{\lambda} \otimes \vec{a}_{\mu}) = -2T_{\mu\lambda}\Delta^{(+)}\vec{a}_{\lambda} \otimes \Delta^{(-)}\vec{a}_{\mu}, \quad (\text{A7f})$$

$$(\bar{v}_{\lambda\mu}^*)_{\times}(\vec{a}_{\lambda} \otimes \vec{a}_{\mu}) = -2T_{\lambda\mu}^*\Delta^{(-)}\vec{a}_{\lambda} \otimes \Delta^{(+)}\vec{a}_{\mu}, \quad (\text{A7g})$$

$$(\bar{v}_{\mu\lambda}^*)_{\times}(\vec{a}_{\lambda} \otimes \vec{a}_{\mu}) = -2T_{\mu\lambda}^*\Delta^{(+)}\vec{a}_{\lambda} \otimes \Delta^{(-)}\vec{a}_{\mu}, \quad (\text{A7h})$$

$$(\bar{v}_{\lambda\mu})_{\lrcorner} \begin{pmatrix} \vec{a}_{\mu} \\ \vec{a}_{\lambda} \end{pmatrix} = \vec{n}_1 \otimes (2iT_{\lambda\mu}\Delta^{(+)}\vec{a}_{\mu}), \quad (\text{A7i})$$

$$(\bar{v}_{\mu\lambda})_{\lrcorner} \begin{pmatrix} \vec{a}_{\mu} \\ \vec{a}_{\lambda} \end{pmatrix} = 2iT_{\mu\lambda}\Delta^{(+)}\vec{a}_{\lambda} \otimes \vec{n}_1, \quad (\text{A7j})$$

$$(\bar{v}_{\lambda\mu}^*)_{\lrcorner} \begin{pmatrix} \vec{a}_{\mu} \\ \vec{a}_{\lambda} \end{pmatrix} = (-2iT_{\lambda\mu}^*\Delta^{(-)}\vec{a}_{\lambda}) \otimes \vec{n}_2, \quad (\text{A7k})$$

$$(\bar{v}_{\mu\lambda}^*)_{\lrcorner} \begin{pmatrix} \vec{a}_{\mu} \\ \vec{a}_{\lambda} \end{pmatrix} = \vec{n}_2 \otimes (-2iT_{\mu\lambda}^*\Delta^{(-)}\vec{a}_{\mu}), \quad (\text{A7l})$$

where $[\vec{a}_{\lambda}]_k$ and $[\vec{a}_{\mu}]_k$ refer to the k -th component ($k = 1, 2, 3$) in the basis defined by the single-atom Bloch vector $\langle \vec{\sigma}_{\lambda} \rangle = (\langle \sigma_{\lambda}^- \rangle, \langle \sigma_{\lambda}^+ \rangle, \langle \sigma_{\lambda}^z \rangle)^T$, $\vec{n}_1 = (\frac{1}{2}, 0, 0)^T$, $\vec{n}_2 = (0, \frac{1}{2}, 0)^T$, $\vec{0} = (0, 0, 0)^T$, and

$$\Delta^{(-)} = \begin{pmatrix} 0 & 0 & -i/2 \\ 0 & 0 & 0 \\ 0 & i & 0 \end{pmatrix}, \quad \Delta^{(+)} = \begin{pmatrix} 0 & 0 & 0 \\ 0 & 0 & i/2 \\ -i & 0 & 0 \end{pmatrix}. \quad (\text{A8})$$

Identities (A7) show that the blocks of the matrix \bar{v} accomplish mutual mappings between the vectors of the form \vec{p}_1 and \vec{p}_2 (we omit for the moment the indices λ, μ):

$$\bar{v}_{\lrcorner} : \vec{p}_2 \rightarrow \vec{p}'_1, \quad \bar{v}_{\times} : \vec{p}_2 \rightarrow \vec{p}'_2, \quad \bar{v}_{\lrcorner} : \vec{p}_1 \rightarrow \vec{p}'_2, \quad (\text{A9})$$

where \vec{p}'_j ($j = 1, 2$) is the result of the transformation which has the same structure as the vector \vec{p}_j .

Returning to the three-atom case, it can be shown that the matrices U_{α} and W_{α} ($\alpha = \lrcorner, \lrcorner, \times$), acting on the test vectors

$$\vec{P}_1 = (\vec{a}_3, \vec{a}_2, \vec{a}_1)^T, \quad (\text{A10a})$$

$$\vec{P}_2 = (\vec{a}_2 \otimes \vec{a}_3, \vec{a}_1 \otimes \vec{a}_3, \vec{a}_1 \otimes \vec{a}_2)^T, \quad (\text{A10b})$$

$$\vec{P}_3 = \vec{a}_1 \otimes \vec{a}_2 \otimes \vec{a}_3, \quad (\text{A10c})$$

map them to each other according to the transformation rules:

$$U_{\lrcorner} : \vec{P}_2 \rightarrow \vec{P}'_1, \quad U_{\lrcorner} : \vec{P}_1 \rightarrow \vec{P}'_2, \quad U_{\times} : \vec{P}_2 \rightarrow \vec{P}'_3, \quad (\text{A11a})$$

$$W_{\lrcorner} : \vec{P}_3 \rightarrow \vec{P}'_2, \quad W_{\lrcorner} : \vec{P}_2 \rightarrow \vec{P}'_3, \quad W_{\times} : \vec{P}_3 \rightarrow \vec{P}'_3. \quad (\text{A11b})$$

Now, the action of the matrices $(U_{\lambda\mu})_{\alpha}$, $(W_{\lambda\mu})_{\alpha}$, ($\lambda, \mu = 1, 2, 3$) on the vectors \vec{P}_j is fully determined by the action of the matrices $(\bar{v}_{\lambda\mu})_{\alpha}$ on the vectors $(\vec{p}_{\lambda\mu})_1$ and $(\vec{p}_{\lambda\mu})_2$. In other words, the explicit form of the vectors \vec{P}'_j can be obtained by appropriately constructing the three-atom vectors out of the vectors $(\vec{p}'_{\lambda\mu})_1$ and $(\vec{p}'_{\lambda\mu})_2$, the latter vectors being defined in the right hand side of Eqs. (A7).

Vector \vec{P}'_1 is created from the vector $(\vec{p}'_{\lambda\mu})_1$ by appending the null vector $\vec{0}$ at the position corresponding to atom $\beta \neq \lambda \neq \mu$, such that the atomic indices of the resulting vector are arranged in decreasing order, as in the vector \vec{P}_1 . Vector \vec{P}'_2 is created from the vector $(\vec{p}'_{\lambda\mu})_2$ by appending the 2 vectors $\vec{0} \otimes \vec{0}$, such that the atomic indices are arranged in the same order as in vector \vec{P}_2 . Finally, the vector \vec{P}'_3 is created from the vector $(\vec{p}'_{\lambda\mu})_2$ by appending a tensor product with vector \vec{a}_{β} ($\beta \neq \lambda \neq \mu$), such that the atomic indices are arranged in the same order as in the vector \vec{P}_3 .

Appendix B: Integral representations for the Green's functions

From the definitions of Eqs. (A1b) and (14), it follows:

$$G_{\times}(z) = G_{23}(z) \oplus G_{13}(z) \oplus G_{12}(z). \quad (\text{B1})$$

Here, $G_{\lambda\mu}(z)$ is the Green's matrix for two independent atoms λ and μ :

$$G_{\lambda\mu}(z) \equiv (z - M_{\lambda\mu})^{-1}, \quad (\text{B2})$$

where $M_{\lambda\mu}$ is the evolution matrix of two free atoms,

$$M_{\lambda\mu} = M_{\lambda} \otimes \mathbf{1} + \mathbf{1} \otimes M_{\mu}. \quad (\text{B3})$$

As proven in Ref. [23], the Green's matrix $G_{\lambda\mu}(z)$ can be represented as

$$G_{\lambda\mu}(z) = \int_{-\infty}^{\infty} \frac{d\omega'}{2\pi} G_{\lambda} \left(\frac{z}{2} \pm i\omega' \right) \otimes G_{\mu} \left(\frac{z}{2} \mp i\omega' \right), \quad (\text{B4})$$

where $G_{\lambda}(z)$ is defined in Eq. (14). Hence, $G_{\times}(z)$ (cf. Eq. (B1)) is given by a direct sum of three integrals in the form of Eq. (B4).

Using this result, we will show that a similar integral representation can be obtained for the Green's matrix

$$D_{\times}(z) = (z - N_{\times})^{-1}, \quad (\text{B5})$$

governing evolution of three independent atoms. Matrix N_\times , specified in Eq. (A1e), can be written as

$$N_\times = M_1 \otimes \mathbb{1} \otimes \mathbb{1} + \mathbb{1} \otimes M_{23}. \quad (\text{B6})$$

Obviously, N_\times has the same structure as the matrix M_\times , see Eq. (B3). Therefore, we can represent it, by analogy with Eq. (B4), as

$$D_\times(z) = \int_{-\infty}^{\infty} \frac{d\omega'}{2\pi} G_1\left(\frac{z}{2} \pm i\omega'\right) \otimes G_{23}\left(\frac{z}{2} \mp i\omega'\right). \quad (\text{B7})$$

Finally, using the integral representation for the Green's function $G_{23}(z')$:

$$G_{23}(z') = \int_{-\infty}^{\infty} \frac{d\omega''}{2\pi} G_2\left(\frac{z'}{2} \pm i\omega''\right) \otimes G_3\left(\frac{z'}{2} \mp i\omega''\right), \quad (\text{B8})$$

where $z' \equiv z/2 \mp i\omega'$, we obtain

$$D_\times(z) = \int_{-\infty}^{\infty} \int_{-\infty}^{\infty} \frac{d\omega'}{2\pi} \frac{d\omega''}{2\pi} G_1\left(\frac{z}{2} \pm i\omega'\right) \otimes G_2\left(\frac{z'}{2} \pm i\omega''\right) \otimes G_3\left(\frac{z'}{2} \mp i\omega''\right), \quad (\text{B9})$$

which yields the integral representation for the function $D_\times(z)$.

Appendix C: Sum rules

The following sum rules constitute a method of calculating exactly sums of the frequency integrals appearing in the expressions for the vectors $\vec{x}^{(n)}$, $\vec{y}^{(n)}$, and $\vec{z}^{(n)}$ due to the integral representations of the matrices $G_\times(z)$ and $D_\times(z)$ given by Eqs. (B4) and (B9), respectively.

The idea of the method is based on the spectral decomposition of the single-atom Green's matrices $G_\lambda(z)$, followed by calculation of the frequency integrals in the complex plane and, finally, a summation of the results. We will outline here the main steps in deriving the sum rules, and illustrate them with two characteristic examples. Further useful, though restricted to the two-atom case, examples can be found in [23].

We will first note that the Bloch matrix M_λ governing the evolution of atom λ (see Eq. (A2)) allows for a spectral decomposition

$$M_\lambda = \sum_k r_k P_k^\lambda, \quad (\text{C1})$$

where

$$P_k^\lambda = \frac{|u_k^\lambda\rangle\langle v_k^\lambda|}{\langle v_k^\lambda|u_k^\lambda\rangle}, \quad \sum_k P_k^\lambda = \mathbb{1}, \quad (\text{C2})$$

is the projector on the subspace corresponding to the eigenvalue r_k , and $|u_k^\lambda\rangle$ ($|v_k^\lambda\rangle$) are the right (left) eigenvectors of the matrix M_λ satisfying $\langle v_k^\lambda|u_{k'}^\lambda\rangle = 0$ for $k \neq k'$

[31]. The eigenvalues r_k of the matrix M_λ are the roots of the characteristic polynomial thereof:

$$f(z) = (z + 2\gamma)((z + \gamma)^2 + \delta^2) + (z + \gamma)|\Omega|^2. \quad (\text{C3})$$

While the explicit form of r_k will be unimportant to us, we will rely on the fact that for arbitrary $|\Omega|$ and δ , the roots are non-degenerate, and $\text{Re}[r_k] < 0$.

To illustrate the sum rules, we will calculate the zeroth-order correlation functions $\vec{y}^{(0)}$ and $\vec{z}^{(0)}$. Although the results are known without any calculations, cf. Eq. (13), we will obtain them alternatively by using the sum rules. These derivations highlight all steps needed for tackling more complicated cases.

Taking $n = 0$ in Eq. (12b), we obtain

$$\vec{y}^{(0)} = G_\times L_+ \vec{x}^{(0)}. \quad (\text{C4})$$

Using Eqs. (A1c), (B1), and (B4), we can bring Eq. (C4) to the form

$$\vec{y}^{(0)} = (\mathcal{G}_{23}, \mathcal{G}_{13}, \mathcal{G}_{12})^T, \quad (\text{C5})$$

where

$$\mathcal{G}_{\lambda\mu} \equiv \int_{-\infty}^{\infty} \frac{d\omega'}{2\pi} \left(G_\lambda(i\omega') \vec{L} \otimes G_\mu(-i\omega') G_\mu \vec{L} + G_\lambda(i\omega') G_\lambda \vec{L} \otimes G_\mu(-i\omega') \vec{L} \right), \quad (\text{C6})$$

and, for definiteness, the upper sign in the integrals (B4) was taken.

Next, inserting into (C6) a spectral decomposition of the single-atom Green's matrix

$$G_\lambda(z) = \sum_k \frac{P_k^\lambda}{z - r_k}, \quad (\text{C7})$$

which follows directly from Eqs. (C1) and (14), we arrive at

$$\mathcal{G}_{\lambda\mu} = \int_{-\infty}^{\infty} \frac{d\omega'}{2\pi} \times \sum_{k,l} \left(\frac{P_k^\lambda}{i\omega' - r_k} \vec{L} \otimes \frac{P_l^\mu}{-i\omega' - r_l} \frac{1}{-r_l} \vec{L} + \frac{P_k^\lambda}{i\omega' - r_k} \frac{1}{-r_k} \vec{L} \otimes \frac{P_l^\mu}{-i\omega' - r_l} \vec{L} \right). \quad (\text{C8})$$

This integral can now easily be taken using the residues theorem. By noting that, in the upper complex half-plane of ω' , the integrand of (C8) has simple poles at $\omega' = -ir_k$, we obtain the result

$$\begin{aligned} \mathcal{G}_{\lambda\mu} &= \sum_{k,l} \left(\frac{P_k^\lambda}{1} \vec{L} \otimes \frac{P_l^\mu}{-r_k - r_l - r_l} \frac{1}{-r_l} \vec{L} + \frac{P_k^\lambda}{-r_k} \vec{L} \otimes \frac{P_l^\mu}{-r_k - r_l} \right) \\ &= \sum_{k,l} \frac{P_k^\lambda}{-r_k} \vec{L} \otimes \frac{P_l^\mu}{-r_l} \vec{L} = G_\lambda \vec{L} \otimes G_\mu \vec{L}, \end{aligned} \quad (\text{C9})$$

whence, in agreement with Eq. (13b), it follows

$$\vec{y}^{(0)} = (G_2 \vec{L} \otimes G_3 \vec{L}, G_1 \vec{L} \otimes G_3 \vec{L}, G_1 \vec{L} \otimes G_2 \vec{L})^T. \quad (\text{C10})$$

We will proceed with a calculation of $\vec{z}^{(0)}$ for which Eq. (12c) yields

$$\vec{z}^{(0)} = D_\times L_\times \vec{y}^{(0)}. \quad (\text{C11})$$

Inserting into (C11) the integral representation (B9) of $D_\times \equiv D_\times(0)$, the definition of L_\times (Eq. (A1d)), as well as the result (C10), we get

$$\begin{aligned} \vec{z}^{(0)} = & \int_{-\infty}^{\infty} \int_{-\infty}^{\infty} \frac{d\omega'}{2\pi} \frac{d\omega''}{2\pi} \left(G_1(i\omega') \vec{L} \otimes G_2(i\omega''_-) G_2 \vec{L} \otimes G_3(-i\omega''_+) G_3 \vec{L} + G_1(i\omega') G_1 \vec{L} \otimes G_2(i\omega''_-) \vec{L} \otimes G_3(-i\omega''_+) G_3 \vec{L} \right. \\ & \left. + G_1(i\omega') G_1 \vec{L} \otimes G_2(i\omega''_-) G_2 \vec{L} \otimes G_3(-i\omega''_+) \vec{L} \right) \equiv \int_{-\infty}^{\infty} \int_{-\infty}^{\infty} \frac{d\omega'}{2\pi} \frac{d\omega''}{2\pi} \mathcal{G}_{123}(\omega', \omega''), \end{aligned} \quad (\text{C12})$$

with $\omega''_{\pm} = \omega'' \pm \omega'/2$. By virtue of the spectral decomposition (C7) the vector function $\mathcal{G}_{123}(\omega', \omega'')$ yields the expression

$$\begin{aligned} \mathcal{G}_{123}(\omega', \omega'') = & \sum_{k,l,m} \left(\frac{P_k^1}{i\omega' - r_k} \vec{L} \otimes \frac{1}{i\omega'' - i\omega'/2 - r_l} \frac{P_l^2}{-r_l} \vec{L} \otimes \frac{1}{-i\omega'' - i\omega'/2 - r_m} \frac{P_m^3}{-\lambda_m} \vec{L} \right. \\ & + \frac{1}{i\omega' - r_k} \frac{P_k^1}{-r_k} \vec{L} \otimes \frac{P_l^2}{i\omega'' - i\omega'/2 - r_l} \vec{L} \otimes \frac{1}{-i\omega'' - i\omega'/2 - r_m} \frac{P_m^3}{-r_m} \vec{L} \\ & \left. + \frac{1}{i\omega' - r_k} \frac{P_k^1}{-r_k} \vec{L} \otimes \frac{1}{i\omega'' - i\omega'/2 - r_l} \frac{P_l^2}{-r_l} \vec{L} \otimes \frac{P_m^3}{-i\omega'' - i\omega'/2 - r_m} \vec{L} \right). \end{aligned} \quad (\text{C13})$$

Taking integral over ω'' in the complex plane, we observe that each of the lines of (C13) has a simple pole $\omega'' = -ir_l + \omega'/2$ in the upper half-plane (and, also, $\omega'' = ir_m + \omega'/2$ - in the lower half-plane), which gives

$$\begin{aligned} \int_{-\infty}^{\infty} \frac{d\omega''}{2\pi} \mathcal{G}_{123}(\omega', \omega'') = & \sum_{k,l,m} \left(\frac{P_k^1}{i\omega' - r_k} \vec{L} \otimes \frac{P_l^2}{-r_l} \vec{L} \otimes \frac{1}{-i\omega' - r_l - r_m} \frac{P_m^3}{-r_m} \vec{L} \right. \\ & + \frac{1}{i\omega' - r_k} \frac{P_k^1}{-r_k} \vec{L} \otimes \frac{P_l^2}{1} \vec{L} \otimes \frac{1}{-i\omega' - r_l - r_m} \frac{P_m^3}{-r_m} \vec{L} \\ & \left. + \frac{1}{i\omega' - r_k} \frac{P_k^1}{-r_k} \vec{L} \otimes \frac{P_l^2}{-r_l} \vec{L} \otimes \frac{P_m^3}{-i\omega' - r_l - r_m} \vec{L} \right). \end{aligned} \quad (\text{C14})$$

Finally, the integral over ω' yields

$$\begin{aligned} \vec{z}^{(0)} = & \sum_{k,l,m} \left(\frac{P_k^1}{1} \vec{L} \otimes \frac{P_l^2}{-r_l} \vec{L} \otimes \frac{1}{-r_k - r_l - r_m} \frac{P_m^3}{-r_m} \vec{L} + \frac{P_k^1}{-r_k} \vec{L} \otimes \frac{P_l^2}{1} \vec{L} \otimes \frac{1}{-r_k - r_l - r_m} \frac{P_m^3}{-r_m} \vec{L} \right. \\ & \left. + \frac{P_k^1}{-r_k} \vec{L} \otimes \frac{P_l^2}{-r_l} \vec{L} \otimes \frac{P_m^3}{-r_k - r_l - r_m} \vec{L} \right) = \sum_{k,l,m} \frac{P_k^1}{-r_k} \vec{L} \otimes \frac{P_l^2}{-r_l} \vec{L} \otimes \frac{P_m^3}{-r_m} \vec{L} = G_1 \vec{L} \otimes G_2 \vec{L} \otimes G_3 \vec{L}, \end{aligned} \quad (\text{C15})$$

which confirms Eq. (13c).

It should be mentioned that the sum rules are valid also in a more general case when the detunings and/or Rabi frequencies depend upon the atomic index λ . Indeed, the fact that the eigenvalues r_k^λ in these cases depend on λ changes nothing in the preceding derivations. That means that the results obtained in this paper can be generalized to include, e.g., residual thermal motion of atoms via individual Doppler shifts and, hence, de-

tunings δ_λ , or wave propagation in the effective medium, in which case the laser field strength (Rabi frequency) would depend on the atomic position inside the medium.

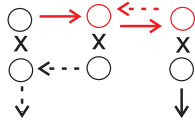


FIG. 23: (Color online) Diagram (c1)(f1)(d2) contains an amplitude that comes in and cycles between the circles (highlighted with red) without the outgoing arrow.

Appendix D: Forbidden diagrams

1. Combinations of diagrams from Fig. 10

The following combinations are forbidden: (c1)(f1)(d2), (c1)(f4)(d2), (c2)(f1)(d2), (c2)(f2)(d1),

(c2)(f2)(d2), (c2)(f2)(d3), (c2)(f3)(d2), (c2)(f4)(d1), (c2)(f4)(d2), (c2)(f4)(d3), (c2)(f5)(d2), (c3)(f1)(d2), (c3)(f4)(d2). All these diagrams as well as the ones listed below contain closed loops (see an example in Fig. 23).

2. Combinations of diagrams from Fig. 12

(a1)(g4)(d2), (a1)(g5)(d2), (a1)(g6)(d2), (a1)(g8)(d2), (a2)(g4)(d2), (a2)(g5)(d2), (a2)(g6)(d2), (a2)(g8)(d2).

-
- [1] M. P. Van Albada and A. Lagendijk, *Phys. Rev. Lett.* **55**, 2692 (1985); P.-E. Wolf and G. Maret, *Phys. Rev. Lett.* **55**, 2696 (1985); Y. Kuga and A. Ishimaru, *J. Opt. Soc. Am. A* **1**, 831 (1984).
- [2] G. Labeyrie, F. de Tomasi, J.-C. Bernard, C. A. Müller, C. Miniatura, and R. Kaiser, *Phys. Rev. Lett.* **83**, 5266 (1999).
- [3] P. Kulatunga, C. I. Sukenik, S. Balik, M. D. Havey, D. V. Kupriyanov, and I. M. Sokolov, *Phys. Rev. A* **68**, 033816 (2003).
- [4] G. Labeyrie, D. Delande, C. A. Müller, C. Miniatura, and R. Kaiser, *Europhys. Lett.* **61**, 327 (2003).
- [5] T. Chanelière, D. Wilkowski, Y. Bidet, R. Kaiser, and C. Miniatura, *Phys. Rev. E* **70**, 036602 (2004).
- [6] S. Balik, P. Kulatunga, C. I. Sukenik, M. D. Havey, D. V. Kupriyanov, and I. M. Sokolov, *J. Mod. Opt.* **52**, 2269 (2005).
- [7] E. Akkermans, A. Gero, and R. Kaiser, *Phys. Rev. Lett.* **101**, 103602 (2008).
- [8] I. M. Sokolov, M. D. Kupriyanova, D. V. Kupriyanov, and M. D. Havey, *Phys. Rev. A* **79**, 053405 (2009).
- [9] T. Savels, A. P. Mosk, and A. Lagendijk, *Phys. Rev. Lett.* **98**, 103601 (2007).
- [10] A. Goetschy and S. E. Skipetrov, *Europhys. Lett.* **96**, 34005 (2011).
- [11] C. A. Müller and C. Miniatura, *J. Phys. A* **35**, 10163 (2002).
- [12] D. V. Kupriyanov, I. M. Sokolov, P. Kulatunga, C. I. Sukenik and M. D. Havey, *Phys. Rev. A* **67**, 013814 (2003).
- [13] T. Wellens, B. Grémaud, D. Delande, and C. Miniatura, *Phys. Rev. A* **73**, 013802 (2006).
- [14] G. S. Agarwal, *Quantum Statistical Theories of Spontaneous Emission and their Relation to Other Approaches*, (Springer, Berlin, 1974).
- [15] C. Cohen-Tannoudji, J. Dupont-Roc, and G. Grynberg, *Atom-Photon Interactions*, Ch. V (Wiley-VCH, Weinheim, 2004).
- [16] R. H. Lehmberg, *Phys. Rev. A* **2**, 883 (1970).
- [17] V. Shatokhin, C. A. Müller, and A. Buchleitner, *Phys. Rev. Lett.* **94**, 043603 (2005).
- [18] V. Shatokhin, C. A. Müller, and A. Buchleitner, *Phys. Rev. A* **73**, 063813 (2006).
- [19] B. Grémaud, T. Wellens, D. Delande, C. Miniatura, *Phys. Rev. A* **74**, 033808 (2006).
- [20] V. Shatokhin, T. Wellens, B. Grémaud, and A. Buchleitner, *Phys. Rev. A* **76**, 043832 (2007).
- [21] T. Wellens, T. Geiger, V. Shatokhin, and A. Buchleitner, *Phys. Rev. A* **82**, 013832 (2010).
- [22] T. Geiger, T. Wellens, V. Shatokhin, and A. Buchleitner, *Photon. Nanostr. Fund. Appl.* **8**, 244 (2010).
- [23] V. Shatokhin, T. Geiger, T. Wellens, and A. Buchleitner, *Chem. Phys.* **375**, 150 (2010).
- [24] V. Shatokhin, T. Wellens, and A. Buchleitner, Preprint as <http://arxiv.org/abs/1204.1512> (2012).
- [25] P. Sheng, *Introduction to Wave Scattering, Localization and Mesoscopic Phenomena* (Academic Press, San Diego, 1995).
- [26] We will deal with the inelastic scattering processes whereupon the outgoing wave number may differ from the incident one. However, the associated relative changes are negligibly small and are ignored throughout this work.
- [27] T. Wellens and B. Grémaud, *J. Phys. B: At. Mol. Opt. Phys.* **39**, 4719 (2006).
- [28] B. R. Mollow, *Phys. Rev.* **188**, 1969 (1969).
- [29] B. R. Mollow, *Phys. Rev.* **5**, 2217 (1972).
- [30] T. Wellens and B. Grémaud, *Phys. Rev. Lett.* **100**, 033902 (2008).
- [31] R.A. Horn, C.R. Johnson, *Matrix Analysis*, (Cambridge University Press, Cambridge, 1985).